AD-A129 097 INSTABILITY OF THE FLOW OF IMMISCIBLE LIQUIDS WITH DIFFERENT VISCOSITIES I..(U) WISCONSIN UNIV-MADISON MATHEMATICS RESEARCH CENTER D D JOSEPH ET AL. APR 83 1/1

UNCLASSIFIED MRC-TSR-2503 DAAG29-80-C-0041 F/G 20/4 NL

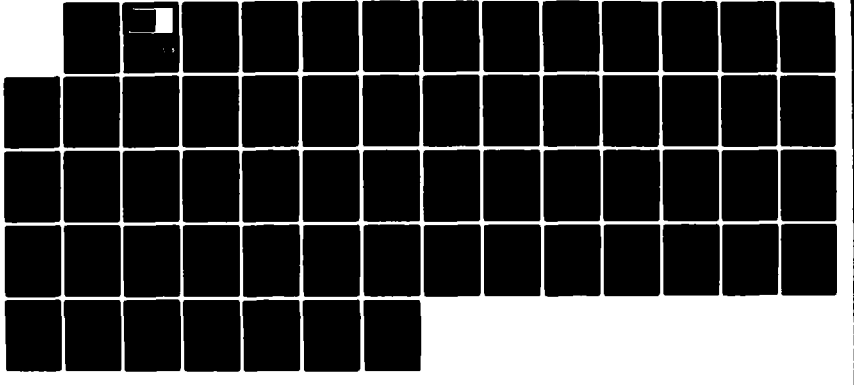

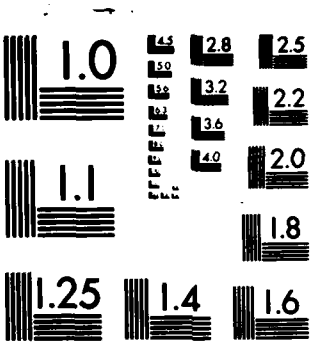

MICROCOPY RESOLUTION TEST CHART
NATIONAL BUREAU OF STANDARDS-1963-A

MRC Technical Summary Report # 2503

INSTABILITY OF THE FLOW OF IMMISCIBLE LIQUIDS WITH DIFFERENT VISCOSITIES IN A PIPE

D. D. Joseph, M. Renardy
and
Y. Renardy

Mathematics Research Center
University of Wisconsin—Madison
610 Walnut Street
Madison, Wisconsin 53706

April 1983

(Received March 7, 1983)

Sponsored by

U. S. Army Research Office
P. O. Box 12211
Research Triangle Park
North Carolina 27709

National Science Foundation
Washington, DC 20550

SECURITY CLASSIFICATION OF THIS PAGE (When Data Entered)

REPORT DOCUMENTATION PAGE		READ INSTRUCTIONS BEFORE COMPLETING FORM
1. REPORT NUMBER #2503	2. GOVT ACCESSION NO. AD-A129097	3. RECIPIENT'S CATALOG NUMBER
4. TITLE (and Subtitle) Instability of the Flow of Immiscible Liquids with Different Viscosities in a Pipe		5. TYPE OF REPORT & PERIOD COVERED Summary Report - no specific reporting period 6. PERFORMING ORG. REPORT NUMBER
7. AUTHOR(s) D. D. Joseph, M. Renardy and Y. Renardy		8. CONTRACT OR GRANT NUMBER(s) MCS-7927062, Mod. 2 DAAG29-80-C-0041
9. PERFORMING ORGANIZATION NAME AND ADDRESS Mathematics Research Center, University of Wisconsin 610 Walnut Street Madison, Wisconsin 53706		10. PROGRAM ELEMENT, PROJECT, TASK AREA & WORK UNIT NUMBERS Work Unit Number 2 - Physical Mathematics
11. CONTROLLING OFFICE NAME AND ADDRESS See Item 18 below		12. REPORT DATE April 1983 13. NUMBER OF PAGES 56
14. MONITORING AGENCY NAME & ADDRESS(if different from Controlling Office)		15. SECURITY CLASS. (of this report) UNCLASSIFIED 15a. DECLASSIFICATION/DOWNGRADING SCHEDULE

16. DISTRIBUTION STATEMENT (of this Report)

Approved for public release; distribution unlimited.

17. DISTRIBUTION STATEMENT (of the abstract entered in Block 20, if different from Report)

18. SUPPLEMENTARY NOTES

U. S. Army Research Office
P. O. Box 12211
Research Triangle Park
North Carolina 27709

National Science Foundation
Washington, DC 20550

19. KEY WORDS (Continue on reverse side if necessary and identify by block number)

Two component flows, interfacial stability, variational principles

20. ABSTRACT (Continue on reverse side if necessary and identify by block number)

We study the flow of two immiscible fluids of different viscosities and equal density through a pipe under a pressure gradient. This problem has a continuum of solutions corresponding to arbitrarily prescribed interface shapes. The question therefore arises, which of these solutions are stable and thus observable. Experiments have shown a tendency for the thinner fluid to encapsulate the thicker one. This has been "explained" by the viscous dissipation principle, which postulates that the amount of viscous dissipation is minimized for a given flow rate. For a circular pipe, this predicts a concentric

(continued)

ABSTRACT (continued)

configuration with the more viscous fluid located at the core. A linear stability analysis, which is carried out numerically, shows that while this configuration is stable when the more viscous fluid occupies most of the pipe, it is not stable when there is more of the thin fluid. Therefore the dissipation principle does not always hold, and the volume ratio is a crucial factor.

UNIVERSITY OF WISCONSIN - MADISON
MATHEMATICS RESEARCH CENTER

INSTABILITY OF THE FLOW OF IMMISCIBLE LIQUIDS WITH DIFFERENT VISCOSITIES IN A PIPE

D. D. Joseph*, M. Renardy** and Y. Renardy**

Technical Summary Report #2503

April 1983

ABSTRACT

The authors:

We study the flow of two immiscible fluids of different viscosities and equal density through a pipe under a pressure gradient. This problem has a continuum of solutions corresponding to arbitrarily prescribed interface shapes. The question therefore arises, which of these solutions are stable and thus observable. Experiments have shown a tendency for the thinner fluid to encapsulate the thicker one. This has been "explained" by the viscous dissipation principle, which postulates that the amount of viscous dissipation is minimized for a given flow rate. For a circular pipe, this predicts a concentric configuration with the more viscous fluid located at the core. A linear stability analysis, which is carried out numerically, shows that while this configuration is stable when the more viscous fluid occupies most of the pipe, it is not stable when there is more of the thin fluid. Therefore the dissipation principle does not always hold, and the volume ratio is a crucial factor.

AMS (MOS) Subject Classifications: 49A21, 76E05, 76T05.
Key Words: Two component flows, interfacial stability, variational principles
Work Unit Number 2 - Physical Mathematics

---

* Department of Aerospace Engineering and Mechanics, 107 Akerman Hall, University of Minnesota, Minneapolis, MN 55455.
** Mathematics Research Center, University of Wisconsin, Madison, WI 53705.

---

*,** Sponsored by the United States Army under Contract No. DAAG29-80-C-0041.
** This material is based upon work supported by the National Science Foundation under Grant No. MCS-7927062, Mod 2.

SIGNIFICANCE AND EXPLANATION

When two immiscible fluids of different viscosities and nearly equal densities flow through a pipe under a pressure gradient, experiments have suggested that no matter what the initial configuration, the less viscous fluid eventually encapsulates the more viscous fluid. This property has been observed for both low and high Reynolds number. For example, in the pipeline transport of viscous oils, the pressure gradient can be reduced by adding water because it tends to coat the pipe wall. Another example arises in the spinning of bicomponent fibers such as nylons, when two polymer melts are extruded through a tube.

Mathematically, anti-planar shear flow (exclusively axial flow with only one non-zero component of velocity which depends on the coordinates perpendicular to the axial coordinate) at low Reynolds number in a cylindrical pipe of arbitrary cross-section has a continuum of solutions: for any pre-assigned interface shape there is a possible flow. Previous theoretical attempts to account for the unique observed flow have relied on the 'viscous dissipation principle' which states that the most favored configuration is the one which minimizes viscous energy dissipation for given volume flux. This holds for low Reynolds number one-component flow but has no mathematical basis for bicomponent flows. Rather, we thought that a stability analysis ought to be done. In fact, for axisymmetric flow in a pipe of circular cross-section, linear stability results for long waves have been calculated numerically by Hickox (1971). However, he only computed for the case in which the less viscous fluid is encapsulated by the higher viscosity fluid. He found this case to be unstable at all Reynolds numbers. He did not consider the case in which the more viscous fluid is centrally located to test for the stability predicted by the viscous dissipation principle. We have therefore reconsidered the linear stability problem but without approximations. The results shows that the viscous dissipation principle does not hold and stability depends primarily on the ratio of the radii of the core fluid and the pipe. Some of our results show qualitative similarities with results of Yih (1967) on the stability of plane Couette flow. The instability is due to a mode which is neutrally stable when the viscosities of the two fluids are equal. It is also neutrally stable in the limit as the viscosities become large so that the instability is purely a finite Reynolds number effect. This can also be seen in Hickox's work and provides a reason as to why the viscous dissipation principle is not always in agreement with analysis of stability.

INSTABILITY OF THE FLOW OF IMMISCIBLE LIQUIDS WITH DIFFERENT VISCOSITIES IN A PIPE

D. D. Joseph*, M. Renardy** and Y. Renardy**

1. Introduction

"God is subtle, but not malicious," Einstein

"Mother nature is a bitch," Murphy.

A major problem in the theory of bicomponent flows lies in their nonuniqueness: The position of the interface is one of the unknowns, but the equations of motion may permit an infinite number of different interface configurations. The question thus arises: which interface positions are stable and thus observable? A number of experiments [1-3], [5], [7], [11-14] have shown a tendency for the thinner of the two fluids to move into regions of high shear. This has led to the conjecture that the stable flow can be characterized by a minimization principle [2], [6]. The amount of viscous energy dissipation should be minimized under appropriate constraints.

In this paper, we focus on antiplane shear flow in a cylindrical pipe. This situation has applications in the transport of oil, where the flow rates can be increased by adding some (less viscous) water. Another application arises in the co-extrusion of two polymers, e.g. in the manufacture of nylon fibers [2]. The implications of the "viscous dissipation principle" are discussed in chapter 2. The flow of a single fluid is described by the variational formulation

$$\min_{u \in H_0^1(\Omega)} \int_\Omega \frac{1}{2}\mu(\nabla u)^2 - Gu \quad . \tag{1.1}$$

* Department of Aerospace Engineering and Mechanics, 107 Akerman Hall, University of Minnesota, Minnespolis, MN 55455.

** Mathematics Research Center, University of Wisconsin, Madison, WI 53705.

*,** Sponsored by the United States Army under Contract No. DAAG29-80-C-0041.

** This material is based upon work supported by the National Science Foundation under Grant No. MCS-7927062, Mod. 2.

Here, the velocity has the form $\underline{u} = u(x,y) \cdot \underline{e}_z$, $-G$ is a constant pressure gradient, and Ω is the cross-section of the pipe. For a two-component flow, μ is a discontinuous function of x and y. For each choice of μ, the functional (1.1) has a minimum, leading to a solution of the Navier-Stokes equations. We impose the constraint that the volume occupied by each fluid is given. Thus μ is allowed to vary in a set of functions taking constant values in two regions, whose measures are prescribed. The conjecture expressed in [2], [6] can then be stated as minimizing (1.1) not only with respect to u, but also with respect to μ. This is equivalent to saying that the amount of viscous dissipation (or work, since the two are equal) is minimized for given flow rate, and maximized for given pressure gradient. Alternatively, we may say that the pressure gradient is minimized for given flow rate, or the flow rate maximized for given pressure gradient.

For a general cross-section of the pipe, we do not know whether this variational problem always has a solution. We show that the existence of the minimizer is implied by an a priori estimate on the length of the interface curve, but we do not know how to obtain such an estimate. For a circular pipe, the symmetry leads to an enormous simplification. The minimizer can be constructed explicitly by elementary means. It is a concentric configuration with the more viscous fluid located at the core.

For this case of a circular pipe, we assess the validity of the dissipation principle by performing a linear stability analysis. This is done in chapter 3. The linearized equations are solved numerically by Orszag's [8] method of Fourier-Chebyshev expansions. The linear stability of bicomponent flows was studied previously by Yih [14] and Hickox [4] using perturbation expansions for long waves. Yih studies plane Couette and plane Poiseuille flow with a single flat interface. They did not pose the problem of selection. In these cases the dissipation principle would predict instability for Poiseuille flow, while it gives no prediction for Couette flow. Yih found instability in the case of Poiseuille flow; for Couette flow, the stability depends on the volume ratio of the two fluids. Hickox [4] studied concentric flow in pipes with the less viscous fluid located at the core and finds instability. He does not consider the reverse case where the

more viscous fluid occupies the core as predicted by the dissipation principle. Both Yih and Hickox find that the critical eigenvalue becomes imaginary for zero Reynolds number, hence the stability or instability of the interface is strictly a finite Reynolds number effect. This shows that encapsulation is a nonlinear phenomenon, governed by the Navier-Stokes equations rather than Stokes equations. It may be noted that the Navier-Stokes equations do no arise from a variational principle.

In our computations, we studied stability for both cases in which the less and more viscous fluids are centrally located. The former is always unstable. For the latter, the most important factor was found to be the volume ratio of the two fluids. When the thicker fluid occupies most of the pipe, we find stability as the viscous dissipation principle predicts. However, as the radius of the core is reduced past about $0.7R_2$, where R_2 is the pipe radius, we find instability. This shows that in any event the dissipation principle is not strict. It is perhaps of interest that the solution of design problem (see §10 of [5]) for the thickness of the water layer which will maximize the flux of oil in the core of the pipe is in the region of stability for sufficiently long waves. We find that the critical radius ratio increases with the wave number of the perturbation. In reality, instability of short waves may be suppressed by surface tension, which was not included in our considerations.

The reader may be inclined to think that our results confirm the dissipation principle when the volume ratio is biased towards the more viscous fluid. We feel, however, that great caution is advisable here. The situation we have dealt with has a rotational symmetry, and symmetric solutions to symmetric problems always have a special status. It is thus quite natural that the concentric configuration should be preferred over others in certain situations, whatever the mechanism may be.

On the other hand, we find that the growth rates of the unstable modes for the minimum dissipation case are smaller by one or two orders of magnitude than for the reverse case in which the thin fluid is at the core. Thus the configuration selected by the dissipation principle appears to be at least less unstable than some other interface positions.

2. The dissipation principle

We consider flow in a horizontal cylindrical pipe, whose cross-section Ω is a bounded domain with a smooth boundary. The pipe is occupied by two fluids of equal densities, but different viscosities μ_1 and $\mu_2 > \mu_1$. We study stationary antiplane shear flow, i.e., if x and y denote transverse, and z the longitudinal coordinate, then the velocity field has the form $\underline{u} = u(x,y)\underline{e}_z$. The flow is forced by a given pressure gradient $\text{grad } p = -G\underline{e}_z$. For this situation, the equation of equilibrium reads

$$\text{div}(\mu \nabla u) = -G \tag{2.1}$$

with the boundary condition

$$u = 0 \quad \text{on} \quad \partial\Omega \ . \tag{2.2}$$

Here μ is a step function assuming the values μ_1 and μ_2. On the interface between the two fluids the velocity and shear stress have to be continuous. These two conditions are automatically satisfied, if (2.1) is taken in the distributional sense. These continuity conditions can also be thought to arise as natural boundary conditions. The equations (2.1) and (2.2) are the Euler equations for the variational problem

$$\min_{u \in H_0^1(\Omega)} \int_\Omega \frac{1}{2} \mu (\nabla u)^2 - Gu \ . \tag{2.3}$$

Let us denote the integral expression in (2.3) by $F_\mu(u)$. Since this is a strictly convex functional of u, the following lemma is immediate.

Lemma 2.1: For any $\mu \in L^\infty(\Omega)$ such that $\mu > \varepsilon > 0$, there exist one and only one $u \in H_0^1(\Omega)$, which solves problem (2.3), and hence problem (2.1), (2.2).

This lemma shows that the flow of two fluids has a high degree of nonuniqueness. It says that for any given arrangement of the fluids there is a corresponding flow field. Experimentally, however, certain interface positions are observed, others are not. The question thus arises, which configuration of the interface is stable.

McLean [6] and Everage [2] have suggested that the stable solution may be the one which minimizes (2.3) also with respect to μ, if, say, the volume occupied by each fluid is given. That is, μ is permitted to vary in the class of step functions

$$\Phi = \{\mu_2 + (\mu_1-\mu_2)\chi_{\Omega_1} \mid \Omega_1 \subset \Omega \text{ measurable}, |\Omega_1| = m\}$$

where m is a number which specifies the volume ration and χ_{Ω_1} denotes the characteristic function of Ω_1; i.e., $\chi_{\Omega_1}(\underline{x}) = 1$ when $\underline{x} \in \Omega_1$ and $\chi_{\Omega_1}(\underline{x}) = 0$ otherwise. If we denote by D the rate of viscous dissipation, and by W the mechanical work done by the fluid, then

$$F_\mu(u) = \frac{1}{2} D-W \quad .$$

For any steady flow, we have $D = W$, and hence the flow that minimizes F_μ is the one that maximizes D or W. Also since $W = G\int_\Omega u$, it maximizes $\int_\Omega u$, the volume flux of the fluid.

In general, we have no proof that the problem

$$\min_{u\in H_0^1(\Omega)} F_\mu(u)$$

$$\mu\in\Phi$$

always has a solution. A minimizer does exist, however, if we impose an a priori boundary on the length of the fluid interface. For this purpose, let us define

$$\Phi_L = \{\mu \in \Phi \mid \text{For any } \varepsilon > 0 \text{ there is a set of at most } [L/\varepsilon] + 1$$

$$\text{closed disks of radius } \varepsilon \text{ which completely covers } \partial\Omega_1\} \quad .$$

This condition is a mathematical rigorization of the statement that the length of $\partial\Omega_1$ is less than or equal to $2L$.

Theorem 2.2. (due to M. Renardy)

There exists $\mu^* \in \Phi_L$ and $u \in H_0^1(\Omega)$ such that

$$F_{\mu^*}(u^*) = \min_{\mu\in\Phi_L} \min_{u\in H_0^1(\Omega)} F_\mu(u) \quad .$$

Proof: Let μ^n, u^n be a minimizing sequence. Then clearly $\{u^n\}$ is uniformly bounded in $H_0^1(\Omega)$ and hence has a weakly convergent subsequence. We shall show next that any sequence $\{\mu^n\}$ in Φ_L has an almost everywhere convergent subsequence whose limit is again in Φ_L.

To see this, let $\varepsilon > 0$ be given. For each ϕ^n, we have at most $[L/\varepsilon] + 1$ ε-disks covering $\partial\Omega_1^n$. Denote the centers of these ε-disks by $M_1^n, M_2^n, \ldots, M_{[L/\varepsilon]+1}^n$. We can now extract a subsequence M^{n_k} such that $M_1^{n_k}, M_2^{n_k}, \ldots, M_{[L/\varepsilon]+1}^{n_k}$ converge, say, to $M_1, \ldots, M_{[L/\varepsilon]+1}$. Then, for any fixed δ and k large enough, the boundary of $\Omega_1^{n_k}$ is covered by $(\varepsilon+\delta)$-disks centered at $M_1, \ldots, M_{[L/\varepsilon]+1}$ and thus by a set of measure $\pi(\varepsilon+\delta)^2([L/\varepsilon] + 1)$. The complement of this set consist of finitely many components on each of which the μ^{n_k} are constant for k large enough. Hence we can extract a convergent subsequence there. Repeating this argument for a sequence ε_m such that $\varepsilon_m \to 0$ and using the standard diagonal argument, we find an almost everywhere convergent subsequence of $\{\mu^n\}$. Now assume $\mu^n \in \Phi_L$, $\mu^n \to \mu$ almost everywhere and $\mu \notin \Phi_L$. Then there is some $\varepsilon > 0$ such that the boundary of $\Omega_1(\mu) = \{(x,y) \in \Omega, \mu(x,y) = \mu_1\}$ cannot be covered by $[L/\varepsilon] + 1$ ε-disks. If that is so, then there is a finite number $P_1, P_2, \ldots, P_N$ of points in $\partial\Omega_1(\mu)$ which cannot be covered by $[L/\varepsilon] + 1$ ε-disks. However, for any $\delta > 0$, and any $k = 1, \ldots, N$, there is a point $Q_k^n \in \partial\Omega_1^n$ in the δ-neighborhood of P_k, if n is chosen large enough. Since $\mu^n \in \Phi_L$, it follows that the Q_k^n can be covered by $[L/\varepsilon] + 1$ ε-disks, and hence that P_k are covered by $[L/\varepsilon] + 1$ $\varepsilon+\delta$-disks. Letting $\delta \to 0$, this yields a contradiction. Thus by extracting convergence subsequences, we find $\mu^n \to \mu$ a.e. and $u^n \to u$ weakly in $H_0^1(\Omega)$. It is an easy consequence that $\eta^n = (\mu^n)^{-1} \to \eta = \mu^{-1}$. Moreover there is a sequence v^n of convex combinatins of the u^n such that $v^n \to u$ strongly in $H_0^1(\Omega)$ and $\nabla v^n \to \nabla u$ almost everywhere. Since the functional

$$K(\eta,u) = \int_\Omega \eta^{-1}(\nabla u)^2 - Gu$$

is convex, we have

$$\overline{\lim_{n\to\infty}} K(\tilde{\eta}^n, v^n) \leq \lim_{n\to\infty} K(\eta^n, u^n) \quad ,$$

where $\tilde{\eta}^n$ is an appropriate convex combination of the η^n. According to Fatou's lemma, we have

$$F_\mu(u) = K(\eta,u) \leq \underline{\lim_{n\to\infty}} K(\tilde{\eta}^n, v^n) \leq \lim_{n\to\infty} K(\eta^n, u^n) = \lim_{n\to\infty} F_{\mu^n}(u^n) \quad .$$

This proves that the pair (μ,u) is a minimizer.

For the special case of a circular pipe, an elementary argument is possible. The following modifies an idea of Everage [2]. Let Ω be a circular disk, and let u_0 be the solution of $\Delta u_0 = -G$, $u_0|_{\partial\Omega} = 0$. We put $u = \frac{u_0}{\mu} + \bar{u}$. Then the integral in (2.3) is equal to

$$\int_\Omega \nabla u_0 \nabla u - Gu$$

$$+ \int_{\Omega_2} \frac{1}{2} \mu_2 (\nabla \bar{u})^2 - \frac{1}{2\mu_2} (\nabla u_0)^2$$

$$+ \int_{\Omega_1} \frac{1}{2} \mu_1 (\nabla \bar{u})^2 - \frac{1}{2\mu_1} (\nabla u_0)^2$$

where $\Omega_2 = \Omega \backslash \Omega_1$ is the region occupied by high viscosity fluid. The first of the expressions is zero. The term

$$\int_{\Omega_2} \frac{1}{2\mu_2} (\nabla u_0)^2 + \int_{\Omega_1} \frac{1}{2\mu_1} (\nabla u_0)^2 \text{ is}$$

maximal if Ω_2, the region of higher viscosity, is where $(\nabla u_0)^2$ takes its smallest values; i.e. if Ω_2 is a disk in the center of the pipe. In this case $\partial\Omega_1$ is a line on which u_0 is constant. If we then choose $\bar{u} = 0$ in the outer region, and $\bar{u} = \text{const.}$ in the inner region such that u is continuous, then the continuity of velocity and shear stress across the interface is satisfied. The expression

$$\int_{\Omega_2} \frac{1}{2} \mu_2 (\nabla \bar{u})^2 + \int_{\Omega_1} \frac{1}{2} \mu_1 (\nabla \bar{u})^2$$

becomes zero, which is clearly its minimal value. We have therefore proved

Theorem 2.3.

If Ω is a circular disk, then

$$\min_{\substack{u \in H_0^1(\Omega) \\ \mu \in \Phi}} \int \frac{1}{2} \mu (\nabla u)^2 - Gu$$

is attained for a concentric configuration with the higher viscosity in the inner region.

3. Linear Stability

We consider a circular pipe of radius R_2 and a basic flow given by an axial velocity

$$W_1 = \frac{G}{4\mu_1}\,[m\,R_2^2 + (1-m)R_1^2 - r^2] \qquad 0 \le r \le R_1$$

$$W_2 = \frac{G}{4\mu_2}\,(R_2^2 - r^2) \qquad R_1 \le r \le R_2 \tag{3.1}$$

$$m = \mu_1/\mu_2 \ .$$

Here μ_1, μ_2 are the viscosities of the fluids in the inner and outer region, and G is the applied pressure gradient. We superimpose an infinitesimal disturbance which is periodic in the axial direction and use a Fourier expansion in the azimuthal direction; we therefore represent the disturbance by

$$(u,v,w;p)\exp(-i\alpha ct + i\alpha z + in\theta) \ .$$

where u, v, w denote the radial, azimuthal and axial velocities and p is the pressure. The stability equations are derived from the Navier-Stokes equations plus the conditions that velocities and tractions are continuous at the interface. From these conditions the following eigenvalue problem for c is obtained [4] (for simplicity, we put the density of both fluids equal to 1):

$$\begin{aligned}
i\alpha(W-c)u &= -p' + \mu\Big[\frac{1}{r}(ru')' - \frac{n^2+1}{r^2}u - \alpha^2 u - \frac{2inv}{r^2}\Big] \\
i\alpha(W-c)v &= -\frac{inp}{r} + \mu\Big[\frac{1}{r}(rv')' - \frac{n^2+1}{r^2}v - \alpha^2 v + \frac{2inu}{r^2}\Big] \\
i\alpha(W-c)w + uW' &= -i\alpha p + \mu\Big[\frac{1}{r}(rw')' - \frac{n^2}{r^2}w - \alpha^2 w\Big] \\
(ru)' + inv + ri\alpha w &= 0 \ .
\end{aligned} \tag{3.2}$$

The boundary and interface conditions are

$$
\left.
\begin{aligned}
& u = v = w = 0 \quad \text{at} \quad r = R_2 \\
& [v] = [u] = 0 \\
& [p] = 2[\mu u'] \\
& [\mu v'] + \frac{1}{R_1}(inu - v)[\mu] = 0 \\
& [\mu w'] + i\alpha u[\mu] = 0 \\
& u[W'] + (W - c)i\alpha[w] = 0 \quad .
\end{aligned}
\right\} \qquad \text{at} \quad r = R_1 \tag{3.3}
$$

Here a prime denotes $\frac{d}{dr}$, [ ] denotes the difference between the values of a quantity on both sides of the interface, and W is given by (3.1).

4. Numerical calculations

4.1. Method of calculation

We eliminate w and p from the third and fourth equation in (3.2), so that the problem reduces to finding u and v from the remaining equations and the boundary conditions (3.3). When eliminating w from the fourth equation, we divide by r, thus, even if we impose the condition that u and v are smooth at $r = 0$, we allow w to have an (unphysical) $\frac{1}{r}$ - singularity. The third equation in (3.2) has a regular singular point at 0, and -1 is a root of the indicial equation precisely for $n = 1$. Since the second root is $+1$, the unbounded solution generally behaves like $\frac{1}{r} + ar \ln r$ near $r = 0$. It can be shown that the coefficient a of the logarithmic term vanishes iff $c = W_1(0) - 3\eta_1\alpha i$. This appears in our calculations as an extra eigenvalue for $n = 1$, which must be dismissed as unphysical.

For simplicity, we take the inner radius R_1 equal to 1. We express the radial dependence of the disturbance as a linear combination of Chebyshev polynomials $T_m(r) = \cos(m \arccos r)$ as suggested by Orszag [8] and truncate. Hence the radial velocity is

$$
u = \sum_{m=0}^{N} u_m T_m(r) \qquad 0 \leq r \leq 1
$$

$$
u = \sum_{m=0}^{N} u_m T_m(\bar{r}) \qquad 1 \leq r \leq R_2
$$

where $\bar{r} = -1 + \frac{2(r-1)}{R_2-1}$ ranges from -1 to 1. The terms of highest differential order are r^4u'''' and r^3v''' in the first equation of (3.2) and r^3u''' and r^2v'' in the second equation. We would like the terms u'''' and v''' to be approximated to the same degree. Since we chose u to be an Nth degree polynomial, both terms are of degree $N-4$ if v is a polynomial of degree $N-1$. We thus put

$$v = \sum_{m=0}^{N-1} v_m T_m(r) \qquad 0 \leq r \leq 1$$

$$v = \sum_{m=0}^{N-1} v_m T_m(\bar{r}) \qquad 1 \leq r \leq R_2 \ .$$

If the azimuthal number n is even, then u and v must be odd functions of r (consequently p and w are even), if n is odd, then u and v are even. Consistent with this, the sums in the inner region are restricted to odd (or, resp., even) Chebyshev polynomials. The expressions for u and v are inserted into the equations, which are then truncated at orders $N-4$, $N-3$ resp. For convenience, we take N to be odd. In the outer region, we then have $2N+1$ unknowns and $2N-5$ equations. In the inner region, we get $N+1$ unknowns and $N-2$ equations if n is odd, while we get N unknowns and $N-3$ equations if n is even. Together with the 9 boundary and interface conditions, this yields $3N+2$ (for n odd) or, $3N+1$ (for n even) equations and unknowns.

The eigenvalues c of the resulting matrix equation were computed in complex double precision on a VAX/VMS V02 system using the IMSL routine EIGSC. The flow is unstable if the imaginary part of c is positive.

4.2. Accuracy and convergence

We compared the eigenvalues for the one-fluid case $\mu_1 = \mu_2$ with the results of Salwen and Grosch [9] and Salwen, Cotton and Grosch [10]. For $n = 1$, they list four eigenvalues with the smallest imaginary parts at Reynolds number $Re = \frac{GR_2^3}{4\mu^2} = 100$ and

higher, to 5 decimal places. The velocity scale $\frac{GR_2^2}{4\mu}$ is fixed at 1, and $\alpha R_2 = 1$. We are mainly interested in low Reynolds numbers, so we checked our calculations at $Re = 100$ truncated at $N = 19$ for various values of R_2 to be used in bicomponent flows. A comparison is shown in figure 1. For other azimuthal modes and lower values of Re, our eigenvalues were checked against graphs published by Salwen et al. At best, we can read their graphs to 2 digits, and our results for $N = 19$ agree within that accuracy. Our values for $Re = 10$ and 100 are shown in figures 2 and 3.

Figure 1

$Re = GR_2^3/4\mu^2 = 100$,

Velocity scale $= GR_2^2/4\mu = 1$

mode 1

$\alpha R_2 = 1$

	R_2	μ	c	eigenvalues			
Published by Salwen, Cotton & Grosch	1	.01	.04	.57256,-.14714	.55198,-.37446	.78735,-.47946	.66247,-.74907
Our computation	5	.05	.008	"	"	"	.66248,-.74908
with $N = 19$, $\mu_1 = \mu_2$	2	.02	.02	"	.55199,-.37446	"	.66248,-.74907
	1.25	.0125	.32	.57254,-.14716	.55214,-.37448	.78736,-.47950	.66220,-.74907

Comparison of our one-fluid ($\mu_1 = \mu_2$) eigenvalues with those published by Salwen et al for mode 1 and $Re = 100$.

Figure 2

$R_2 = 1.0$

$\mu_1 = \mu_2 = 0.1\dot{6}$

$R_2 = 1.\dot{6}$

G = 0.24

N = 19

Mode	eigenvalues				
0	.66676,-1.5778	.81338,- 2.6913	.66657,- 5.0195	.72389,- 7.1393	.66666,-10.448
1	.49106,-1.3935	.76202,- 2.8073	.62772,- 4.8498	.70556,- 7.2282	
2	.40791,-2.6274	.76307,- 4.2327	.57022,- 7.0840	.71238,- 9.6639	
3	.36440,-4.0905	.73178,- 5.9084	.53554,- 9.5574	.70101,-12.372	
4	.33513,-5.7962	.69400,- 7.8343	.50882,-12.289	.68325,-15.348	
5	.31324,-7.7438	.65689,-10.006	.48652,-15.281	.66345,-18.587	

Our one-fluid eigenvalues for modes 0 to 5 at Re = 10 which can be compared with published graphs of Salwen et al

Figure 3

Re = 100 αR_2 = 1.0 N=19 $\mu_1=\mu_2$

Mode	R_2	μ	G	eigenvalues					
0	1.25	.0125	.032	.68626,-.27345	.81160,- .28413	.64648, - .45939	.72999, - .73274	.66679, -1.0274	.69394, -1.3568
	•								
	2.0	.02	.02	.68627,-.27345	.81160,- .28413	.64647, - .45937	.72993, - .73276	.66663, -1.0277	.69444, -1.3579
	5.0	.05	.008	"	"	"	"	"	"
2	1.25	.0125	.032	.49400,-.25600	.70711,- .62217	.56483, - .58500	.68056, -1.0059		
	•								
	2.0	.02	.02	.49400,-.25600	.70710,- .62217	.56482, - .58498	.68051, -1.0061		
	5.0	.05	.008	"	.70710,- .62218	.56482, - .58497	.68052, -1.0062		
3	1.25	.0125	.032	.44087,-.39187	.64116,- .71996	.56903, - .89443	.67818, -1.2737		
	•								
	2.0	.02	.02	.44088,-.39189	.64097,- .71991	.56913, - .89404	.67734, -1.2767		
	5.0	.05	.008	"	.64096,- .71990	.56914, - .89402	.67722, -1.2769		
4	1.25	.0125	.032	.40024,-.55701	.62004,- .88366	.53298, -1.1892	.66487, -1.5714		
	•								
	2.0	.02	.02	.40024,-.55701	.62006,- .88365	.53294, -1.1892	.66482, -1.5714		
	5.0	.05	.008	.40023,-.55702	.62007,- .88361	.53301, -1.1892	.66372, -1.5719		
5	1.25	.0125	.032	.36772,-.74937	.59648,-1.0844	.50485, -1.4990	.64873, -1.8911		
	•								
	2.0	.02	.02	,36772,-.74934	.59647,-1.0845	.50473, -1.4986	.64868, -1.8919		
	5.0	.05	.008	"	.59644,-1.0845	.50458, -1.4987	.65052, -1.8920		

Our one-fluid eigenvalues for modes 0 and 2 to 5 at Re = 100 which can be compared with published graphs of Salwen et al.

The instability due to a jump in viscosity is governed by an interfacial mode, which, at $\mu_1 = \mu_2$, is $c = W(R_1)$, as can be seen from the last interface condition in (3.3). The value of c, and in particular its imaginary part, is typically smaller by orders of magnitude than the remaining eigenvalues. Hence c will generally be approximated less well than the other eigenvalues. Since we are mainly interested in the sign of Im c, we are satisfied with 2-digit-accuracy.

Appropriate Reynolds numbers for the inner and outer fluids are Re 1 $= W_1(0)R_1/\mu_1$ and Re 2 $= W_2(R_1)R_2/\mu_2$ respectively. In our figures, Re will denote a reference Reynolds number $W_2(0)R_2/\mu_2$ in analogy with the one-fluid flow, and "velocity scale" will refer to $W_2(0)$. The im(c) is proportional to the velocity scale so we have chosen $W_2(0) = 1$.

Figure 4a to 4e display samples of convergence tests. There are three main features. First, since we used an equal number of modes in the inner and outer regions, we expect convergence rates to worsen as R_1/R_2 moves away from 0.5. Figure 4a compares $R_1/R_2 = 0.5$ with 0.2. At $R_1/R_2 = 0.5$, all modes have converged to at least 2 digits by $N = 19$. At $R_1/R_2 = 0.2$, $N = 39$ is required for similar accuracy for modes 1 to 4. Also, as $R_1/R_2 \to 0$, im(c) $\to 0$ so round-off errors enter. Our method of expansion has an accuracy of infinite order so that once im(c) has converged to 2 digits, convergence to more digits will occur for values of N which are not much larger.

Secondly, at low Re, convergence is worse for the higher modes because im(c) decreases fast in magnitude as mode number increases. Refer to figure 4b for $R_1/R_2 = 0.6$, $\alpha R_2 = 0.1$, Re $= 0.1$. However, computations need not be done for very small Re because im(c) is proportional to Re in the limit as Re $\to 0$. Figure 5 shows that this low Re regime extends up to about Re 1, Re 2 ~ 10, or Re ~ 1 for the values of μ_1/μ_2 we consider. For higher Re (figure 4c) the magnitude of im(c) is similar for all modes. Note that Re 1 increases as μ_1/μ_2 decreases and this accounts for the slower convergence at smaller μ_1/μ_2, (see figure 4d). At Re $= 1000$, the magnitude of the interfacial mode is similar to that of the stable eigenvalues associated with one-fluid flow. Convergence improves for given α and R_1/R_2 as μ_1/μ_2 increases.

Convergence tests
Velocity Scale = 1

Figure 4a

Re = 100 , αR_2 = 1

R_1/R_2	mode	μ_1/μ_2	c N=19	N=23	N=29	N=39
0.5	0	.1	2.3199, -.80908E-1	2.3200, -.80960E-1		
		.34	1.0456, -.99460E-1	1.0456, -.99459E-1		
	5	.8	.75041,-.28395E-3		.75041,-.28385E-3	
		1.2	.74972, .27602E-3		.74972, .27676E-3	
0.2	0	.2	1.1062 ,-.32150E-2		1.1062 ,-.32165E-2	
		.8	.96904,-.24559E-3		.96904,-.24561E-3	
	1	.8	.96209,-.14594E-3	.96234, .445588E-5	.96236, .16157E-4	
		1.2	.95826, .16343E-3	.95806, .44109E-4	.95805, .348776E-4	
	4	.2	1.0021 ,-.53141E-3	(N=25) .96515, .19951E-3	.95995, .11274E-3	.96002, .11325E-3
		.4	1.0432, .80144E-2		.95997,-.54169E-4	.96001,-.53577E-4

Figure 4b

Re = 0.1 , αR_2 = 0.1

R_1/R_2	mode	μ_1/μ_2	c N=19	N=23
0.6	0,1,2	.2 to 2	agree to at least 2 digits for N = 19 & 23.	
	3	.8	.64665, .27404E-6	.64665, .32850E-6
		1.2	.63501,-.12112E-6	.63501,-.98926E-7
	4	.8	.64327, .52384E-7	.64327, .52089E-7
		1.2	.63766, .10883E-7	.63765, .10965E-7

Figure 4c

Re = 1000 αR_2 = 1

R_1/R_2	mode	μ_1/μ_2	c N=19	N=23
0.8	0	.2	.93533,-.21227	1.0734, -.22125
		.4	.47541,-.94439E-1	.47743,-.95378E-1
		.6	.44044,-.28248E-1	.44029,-.28175E-1
	1	.6	.46588, .61055E-1	.46955, .51454E-1
	2	.6	.44054, .39269E-1	.43580, .36565E-1
	3	.6	.42812, .20765E-1	.41937, .26393E-1

Figure 4d

Re = 100 αR_2 = 1

R_1/R_2	mode	μ_1/μ_2	c N=19	N=23
0.9	4	.2	.28227, .41421E-1	.27855, .43170E-1
		.8	.19747, .17079E-2	.19747, .17079E-2
		1.2	.18410,-.72586E-3	.18410,-.72590E-3
0.6	0	.2	.74558, .19535E-1	.74624, .19216E-1
		.4	.67284, .86605E-2	.67283, .86810E-2
		1.2	.63835, .37367E-3	.63835, .37367E-3
	4	.2	.71083, .28060E-1	.71152, .28025E-1
		.4	.65854, .94602E-2	.65853, .94671E-2
		1.2	.63931, .40320E-3	.63931, .40320E-3

Figure 4e

Re = 100 αR_2 = 10

R_1/R_2	mode	μ_1/μ_2	c N=19	N=23
0.6	0	.2	.74558,.19535E-1	.74624,.19216E-1
		.4	.67284,.86605E-2	.67283,.86810E-2
		1.2	.63835,.37367E-3	.63835,.37367E-3
	4	.2	.71083,.28060E-1	.71152,.28025E-1
		.4	.65854,.94602E-2	.65853,.94671E-1
		1.2	.63931,.40320E-3	.63931,.40320E-3
0.9	0	.2	.30635,.23248E-1	.30454,.20957E-1
		.4	.23388,.10908E-1	.23385,.10758E-1
	1	.2	.30903,.23255E-1	.30379,.21445E-1

Re = 1

R_1/R_2	mode	μ_1/μ_2	c N=19	N=23
0.8	0	.2	.38505,.10363E-1	same to all digits

Convergence tests for velocity scale 1, R_1 = 1, c is the interfacial eigenvalue, N is defined in §4.

Figure 5

Table of c

$\alpha R_2 = 1.0$

$R_2 = 1.\dot{6}$

If $\mu_1/\mu_2 = 1$, c = .64

Mode	μ_1/μ_2	Re = 0.1 N=19	Re = 1.0 N=21	Re = 10 N=19	Re = 100 N=19
0	.2	.97455, .10110E-2	.97610, .98976E-2	1.0332, .27546E-1	.95413,-.21492
	.4	.80551, .45676E-4	.80554, .45570E-3	.80832, .36205E-2	.84021,-.44267E-1
	.6	.72214, .26374E-5	.72215, .26330E-4	.72243, .22082E-3	.73259,-.94479E-2
	.8	.67266,-.54430E-6	.67266,-.54465E-5	.67270,-.57955E-4	.67521,-.22710E-2
	1.2	.61692, .78588E-6	.61692, .78581E-5	.61691, .78910E-4	.61608, .10315E-2
	1.4	.59981, .14019E-5	.59981, .14019E-4	.59980, .14047E-3	.59873, .16238E-2
	1.6	.58667, .18428E-5	.58667, .18428E-4	.58666, .18448E-3	.58554, .20042E-2
	1.8	.57630, .21518E-5	.57630, .21518E-4	.57628, .21531E-3	.57519, .22602E-2
	2.0	.56794, .23670E-5	.56794, .23670E-4	.56793, .23678E-3	.56687, .24353E-2
1	.2	.72407, .17313E-2	.72494, .17272E-1	.78572, .12558	.98511, .23978
	.4	.69522, .30367E-3	.69524, .30362E-2	.69752, .29783E-1	.74489, .11063
	.6	.67276, .94515E-4	.67276, .94512E-3	.67257, .93909E-2	.67945, .55521E-1
	.8	.65476, .29109E-4	.65476, .29112E-3	.65461, .28955E-2	.65139, .21604E-1
	1.2	.62768,-.15665E-4	.62768,-.15665E-3	.62778,-.15602E-2	.63404,-.11536E-1
	1.4	.61723,-.25033E-4	.61723,-.25031E-3	.61739,-.24949E-2	.62850,-.18011E-1
	1.6	.60826,-.30972E-4	.60827,-.30971E-3	.60845,-.30891E-2	.62287,-.22317E-1
	1.8	.60048,-.34859E-4	.60048,-.34858E-3	.60067,-.34788E-2	.61731,-.25528E-1
	2.0	.59365,-.37433E-4	.59366,-.37433E-3	.59385,-.37374E-2	.61193,-.28067E-1
2	.2	.70888, .60657E-3	.70902, .60625E-2	.72345, .55710E-1	.84503, .13246
	.4	.68357, .10109E-3	.68358, .10108E-2	.68385, .10050E-1	.70348, .56898E-1
	.6	.66499, .29953E-4	.66499, .29952E-3	.66493, .29844E-2	.66489, .23013E-1
	.8	.65092, .87628E-5	.65092, .87614E-4	.65089, .87317E-3	.64945, .70449E-2
	1.2	.63138,-.42308E-5	.63138,-.42348E-4	.63139,-.42222E-3	.63257,-.33807E-2
	1.4	.62447,-.64090E-5	.62447,-.64119E-4	.62449,-.63940E-3	.62638,-.51337E-2
	1.6	.61886,-.75211E-5	.61886,-.75191E-4	.61890,-.74993E-3	.62117,-.60515E-2
	1.8	.61428,-.80221E-5	.61428,-.80220E-4	.61432,-.80018E-3	.61677,-.64920E-2
	2.	.61051,-.81659E-5	.61051,-.81651E-4	.61054,-.81458E-3	.61305,-.66410E-2
3	.2	.68296, .27177E-3	.68300, .27169E-2	.68732, .26246E-1	.76245, .89782E-1
	.4	.66619, .39952E-4	.66620, .39953E-3	.66629, .39836E-2	.67516, .29410E-1
	.6	.65453, .99384E-5	.65453, .99380E-4	.65452, .99212E-3	.65474, .86695E-2
	.8	.64615, .23872E-5	.64615, .23872E-4	.64615, .23830E-3	.64595, .20913E-2
	1.2	.63540,-.73184E-6	.63540,-.73179E-5	.63540,-.73016E-4	.63551,-.61239E-3
	1.4	.63191,-.83171E-6	.63191,-.83102E-5	.62925,-.66552E-4	.63205,-.66636E-3
	1.6	.62924,-.66815E-6	.62924,-.66772E-5	.62925,-.66552E-4	.62935,-.49264E-3
	1.8	.62719,-.39763E-6	.62719,-.39772E-5	.62719,-.39521E-4	.62726,-.22735E-3
	2.0	.62561,-.89712E-7	.62561,-.89892E-6	.62561,-.87785E-5	.62562, .68179E-4

4	.2	.66341, .13683E-3	.66343, .13681E-2	.66498, .13444E-1	.71072, .62508E-1
	.4	.65379, .17334E-4	.65379, .17333E-3	.65383, .17307E-2	.65797, .14803E-1
	.6	.64742, .32618E-5	.64742, .32458E-4	.64742, .32430E-3	.64782, .30518E-2
	.8	.64306, .45984E-6	.64306, .45578E-5	.64306, .45530E-4	.64314, .43059E-3
	1.2	.63781, .15272E-6	.63781, .15230E-5	.63781, .15210E-4	.63774, .15003E-3
	1.4	.63623, .47025E-6	.63623, .45816E-5	.63623, .45795E-4	.63609, .44746E-3
	1.6	.63507, .78229E-6	.63507, .77923E-5	.63507, .77896E-4	.63487, .75968E-3
	1.8	.63422, .10623E-5	.63422, .10719E-4	.63422, .10717E-3	.63398, .10450E-2
	2.0	.63360, .13254E-5	.63360, .13250E-4	.63359, .13246E-3	.63332, .12923E-2
5	.2	.65156, .74044E-4	.65157, .74037E-3	.65219, .73338E-2	.67915, .43435E-1
	.4	.64662, .81220E-5	.64662, .81221E-4	.64664, .81155E-3	.64867, .74795E-2
	.6	.64348, .99672E-6	.64348, .99758E-5	.64349, .99752E-4	.64381, .99102E-3
	.8	.64141,-.61500E-7	.64141,-.62222E-6	.64141,-.62150E-5	.64151,-.50575E-4
	1.2	.63902, .28391E-6	.63902, .28294E-5	.63902, .28284E-4	.63895, .27092E-3
	1.4	.63833, .57393E-6	.63833, .57542E-5	.63833, .57520E-4	.63821, .55426E-3
	1.6	.63785, .82756E-6	.63785, .82709E-5	.63784, .82668E-4	.63769, .79957E-3
	1.8	.63750, .10328E-5	.63750, .10305E-4	.63750, .10302E-3	.63731, .99913E-3
	2.0	.63725, .11877E-5	.63725, .11907E-4	.63725, .11904E-3	.63705, .11570E-2

Table of interfacial eigenvalues c at moderate αR_2, showing the linear behaviour of c for small Re.

Figure 6

$\alpha R_2 = 0.1$

Vel. scale = 1

$R_2 = 1.\dot{6}$

If $\mu_1/\mu_2 = 1$, c = .64

Mode	μ_1/μ_2	Re = 0.1 N=23	Re = 1.0 N=21	Re = 100 N=19
0	.2	1.0278, .76832E-4	1.0279, .76813E-3	1.0789, .11537E-1
	.4	.82497, .15796E-5	.82497, .15794E-4	.82722, .83375E-3
	.6	.73040,-.34319E-6	.73040,-.34314E-5	.73063,-.37759E-3
	.8	.67567,-.18262E-6		.67571,-.18566E-3
	1.2	.61490, .11602E-6	.61490, .11599E-5	.61489, .11630E-3
	1.4	.59629, .18666E-6	.59629, .18676E-5	.59628, .18703E-3
	1.6	.58193, .23024E-6	.58193, .23056E-5	.58192, .23076E-3
	1.8	.57052, .25857E-6	.57052, .25819E-5	.57051, .25833E-3
	2.	.56123, .27578E-6	.56123, .27584E-5	.56122, .27594E-3
1	.2	.73041, .13880E-3	.73041, .13880E-2	.76520, .12215
	.4	.69982, .28355E-4	.69982, .28352E-3	.69829, .28183E-1
	.6	.67567, .99696E-5	.67567, .99666E-4	.67466, .98113E-2
	.8	.65614, .33240E-5	.65614, .33213E-4	.65578, .32720E-2
	1.2	.62645,-.19352E-5	.62645,-.19351E-4	.62664,-.19164E-2
	1.4	.61491,-.31559E-5	.61491,-.31547E-4	.61519,-.31310E-2
	1.6	.60496,-.39554E-5	.60496,-.39567E-4	.60529,-.39337E-2
	1.8	.59629,-.44965E-5	.59629,-.44962E-4	.59664,-.44759E-2
	2.	.58868,-.48594E-5	.58868,-.48624E-4	.58903,-.48453E-2
2	.2	.71491, .59674E-4	.71491, .59677E-3	.72743, .56125E-1
	.4	.68751, .10552E-4	.68751, .10551E-3	.68756, .10494E-1
	.6	.66732, .33122E-5	.66732, .33119E-4	.66720, .32953E-2
	.8	.65196, .10125E-5	.65196, .10128E-4	.65192, .10079E-2
	1.2	.63050,-.51817E-6	.63050,-.51952E-5	.63053,-.51756E-3
	1.4	.62285,-.80342E-6	.62285,-.80441E-5	.62289,-.80154E-3
	1.6	.61661,-.96244E-6	.61661,-.96187E-5	.61666,-.95903E-3
	1.8	.61148,-.10455E-5	.61148,-.10459E-4	.61153,-.10426E-2
	2.	.60722,-.10832E-5	.60722,-.10834E-4	.60727,-.10805E-2
3	.2	.68607, .27340E-4	.68607, .27346E-3	.69023, .26512E-1
	.4	.66817, .41653E-5	.66817, .41374E-4	.66825, .41265E-2
	.6	.65566, .89912E-6	.65566, .10766E-4	.65565, .10702E-2
	.8	.64665, .32850E-6	.64665, .26992E-5	.64664, .26945E-3
	1.2	.63501,-.98926E-7	.63501,-.94725E-6	.63501,-.93331E-4
	1.4	.63121,-.10326E-6	.63121,-.11566E-5	.63121,-.11630E-3
	1.6	.62829,-.17003E-6	.62829,-.11025E-5	.62829,-.10835E-3
	1.8	.62603,-.27977E-6	.62603,-.84066E-6	.62604,-.86494E-4
	2.	.62428,-.49064E-7	.62428,-.51888E-6	.62429,-.58743E-4

4	.2	.66492, .13824E-4	.66492, .13822E-3	.66646, .13596E-1
	.4	.65470, .17762E-5	.65470, .17805E-4	.65474, .17759E-2
	.6	.64792, .34729E-6	.64792, .34475E-5	.64792, .34413E-3
	.8	.64327, .52089E-7	.64327, .52700E-6	.64327, .52621E-4
	1.2	.63765, .10965E-7	.63766, .11257E-6	.63765, .11216E-4
	1.4	.63595, .43785E-7	.63595, .39803E-6	.63595, .39672E-4
	1.6	.63470, .68450E-7	.63470, .71858E-6	.63470, .70698E-4
	1.8	.63379, .98872E-7	.63379, .97451E-6	.63378, .99373E-4
	2.	.63311, .13359E-6	.63311, .12566E-5	.63311, .12454E-3

Table of interfacial eigenvalues at moderate Re, showing the linear behaviour of c for small αR_2 and α Re.

Thirdly, we have checked with Hickox's figure 2 (1971) where α is small. Hickox showed that given μ_1/μ_2 and R_1/R_2 and small enough α, results for any Re can be deduced from calculations at one value of Re; namely that im(c) is proportional to $\alpha \times$ Reynolds number and real (c) is not. His figure 2 shows that im(c) versus $R_1/R_2 < 1$ for selected values of $\mu_1/\mu_2 < 1$ for modes 0 and 1. The qualitative behaviour in figure 6 agrees with Hickox's graph. Direct comparison can be made at $\mu_1/\mu_2 = 0.2$. In his notation, our im(c) is $\alpha(c_1/i)W_1(0)$. He computes $(c_1/iR) \times 10^4$ where $R = W_1(0)R_1/\nu_1$ so that with our values at Re = 0.1, $\mu_1/\mu_2 = 0.2$, $R_1/R_2 = 0.6$ in figure 6, we obtain $(c_1/iR) \times 10^4 = 7.17$ for mode 0 and 13 for mode 1 which agree with his graph. The deviation from linearity in Re at small μ_1/μ_2 and Re = 100 is due to the fact that Hickox's result is a "small $\alpha \times$ Reynolds number" result. Thus his application to oil-water flows when the Reynolds number is of order 10^5 would require extremely small α.

For large αR_2, the response is very similar for all modes so that convergence tests are done for one or two modes. See figure 4e. The im(c) is largest at $\mu_1/\mu_2 = .2$ where convergence is worst for our range.

5. Results

When the Reynolds number is zero, we can neglect the left hand side of the first three equations in (3.2). Then c occurs only in the interface condition (3.3). By substituting $\tilde{v} = iv$, $\tilde{w} = iw$, we can make the equations (3.2), (3.3) real, and since c is a simple eigenvalue, it must be real. Thus Im c vanishes as Re $\to$ 0. Moreover, the equations are invariant under the change $\mu \to \lambda\mu$, $p \to \lambda p$, $c \to \lambda c$, $W \to \lambda W$ for any positive factor λ. Therefore, if the velocity scale and μ are changed by the same factor to keep Re fixed, c is proportional to the velocity scale. At low Reynolds number, therefore, Re c is proportional to the velocity scale, while Im c is proportional to the velocity scale times the Reynolds number. Since we have normalized the velocity scale, we have Im c ~ Re, while Re c tends to a finite limit as Re $\to$ 0. This behaviour of the interfacial mode is very different from that of the remaining eigenvalues, which are

proportional to $\frac{1}{Re}$ as $Re \to 0$. At very low Reynolds numbers, this leads to severe numerical problems; however, it seems that we can make Re small enough to be in the "linearized" range (cf. chapter 4).

On all graphs, dark points represent computed values and lines which join them are interpolants. Solid lines are sometimes used to avoid confusion but they are also interpolants. Numbers printed next to the curves denote the azimuthal mode number except on graphs 7 to 11 where they denote the ratio $\frac{\mu_1}{\mu_2}$. In all graphs, the velocity scale is unity. On all graphs, except for graphs 12 and 25, the vertical axis measures the imaginary part of the interfacial eigenvalue c.

Moderate αR_2 (~ 1), moderate Re (~ 100), $\mu_1/\mu_2 \in [0.2,2]$

The sign of im (c) at given R_1/R_2, μ_1/μ_2 does not appear to be very sensitive to changes in αR_2 or Re. For example, at $R_2 = 1.\dot{6}$, compare $Re = 1$, $\alpha = 0.06$ (graph 1) $Re = 1$, $\alpha = 0.6$ (graph 2), $Re = 10$, $\alpha = 0.6$ (graph 3) and $Re = 100$, $\alpha = 0.6$ (graph 4). At $R_2 = 1.25$, $\alpha = 0.8$, compare $Re = 1$ and 100 (graphs 5, 6).

The crucial parameters determining the sign of im(c) are R_1/R_2 and μ_1/μ_2.

Graphs 7 to 11 display the behaviour of *im (c) for modes 0 to 4 at* $Re = 100$ as a function of R_1/R_2, keeping $\frac{\mu_1}{\mu_2}$ constant. Note that in many cases, modes 0 to 4 are not simultaneously stable or unstable. Im (c) decreases to 0 as R_1/R_2 decreases from 0.5 to 0 or increases from 0.9 to 1.0. On graph 7, the curve for $\frac{\mu_1}{\mu_2} = 0.2$ is plotted from tracking the interfacial eigenvalue from $R_1/R_2 = 0.9$. There is a degeneracy for mode 0 between $R_1/R_2 = 0.5$ and 0.6 and between $\frac{\mu_1}{\mu_2} = 0.2$ and 0.4 so that when the eigenvalue is tracked at $R_1/R_2 = 0.5$ from $\frac{\mu_1}{\mu_2} = 1$ down to 0.2 (figure 7) and then at $\frac{\mu_1}{\mu_2} = 0.2$ from $R_1/R_2 = 0.5$ to 0.9 (figure 8) we arrive at a different eigenvalue than if we follow it at $R_1/R_2 = 0.9$ from $\frac{\mu_1}{\mu_2} = 1$ down to 0.2. Tracking the interfacial eigenvalue for $R_1/R_2 > 0.6$ as in figure 9 yields values in column c_2 in figure 8.

Figure 7

$R_1/R_2 = 0.5$, Re = 100 , $\alpha R_2 = 1$, Mode 0

The first column tracks the interfacial eigenvalue c from its value at $\mu_1/\mu_2 = 1$ down to $\mu_1/\mu_2 = 0.2$.

The second column tracks a one-fluid eigenvalue c_{SG} recorded by Salwen and Grosch for $\mu_1/\mu_2 = 1$.

Truncation of Chebyshev polynomials is at N = 19[#]

$\frac{\mu_1}{\mu_2}$	c	c_{SG}
1.0	.75 , 0	.81160,-.28413
.98	.75272,-.28882E-3	.81567,-.28105
.96	.75556,-.59808E-3	.81988,-.27791
.94	.75851,-.92971E-3	.82322,-.27471
.92	.76159,-.12859E-2	.82872,-.27146
.9	.76481,-.16692E-2	.83337,-.26815
.88	.76817,-.20822E-2	.83819,-.26478
.86	.77169,-.25283E-2	.84319,-.26136
.84	.77538,-.30110E-2	.84838,-.25788
.8	.78330,-.41033E-2	.85938,-.25078
.6	.83885,-.14116E-1	.93110,-.21345
.52	.87350,-.22825E-1	.97118,-.19946
.5	.88404,-.25920E-1	.98254,-.19639
.48	.89557,-.29567E-1	.99445,-.19362
.46	.90825,-.33918E-1	1.0068 ,-.19123
.44	.92234,-.39186E-1	1.0196 ,-.18933
.42	.93815,-.45686E-1	1.0322 ,-.18807
.4	.95619,-.53912E-1	1.0440 ,-.18751
.38	.97740,-.64703E-1	1.0531 ,-.18740
.36	1.0040 ,-.79646E-1	1.0551 ,-.18568
.34	1.0456 ,-.99460E-1	1.0389 ,-.17766
.32	1.1013 ,-.98510E-1	1.0100 ,-.18494
.3	1.1483 ,-.90943E-1	.99625,-.19537
.28	1.1953 ,-.84391E-1	.99031,-.20426
.26	1.246 ,-.78904E-1	.98896,-.21315
.25	1.2734 ,-.76548E-1	.98945,-.21787
.24	1.3027 ,-.74462E-1	.99050,-.22279
.22	1.3682 ,-.71192E-1	.99400,-.23322
.2	1.4458 ,-.69373E-1	.99928,-.24428

[#]Convergence was tested at $\mu_1/\mu_2 = 0.34$.

Figure 8

$$\frac{\mu_1}{\mu_2} = 0.2 \quad , \quad Re = 100 \quad , \quad \alpha R_2 = 1 \quad , \quad \text{Mode } 0$$

The first column c_1 shows the behaviour of the eigenvalue which was tracked from the interfacial eigenvalue in Figure 7 for $R_1/R_2 = 0.5$.

For $R_1/R_2 > 0.6$, the eigenvalue which is tracked from the interfacial eigenvalue, for example in Figure 7 and 9, lie in column c_2.

R_1/R_2	c_1	c_2
0.5	1.4458,-.69373E-1	.99928,-.24428
0.52	1.4632,-.77384E-1	.98996,-.24079
0.54	1.4788,-.86497E-1	.98087,-.23635
.6	1.515 ,-.12375	.95413,-.21492
.65	1.5391,-.17317	.92814,-.18215
.68	1.5576,-.21326	.90574,-.15303
.7	1.5747,-.24298	.88523,-.13000
.72	1.5966,-.27278	.85914,-.10415
.75	1.6388,-.31302	.80715,-.64169E-1
.76	1.6551,-.32463	.78624,-.51010E-1
.78	1.6906,-.34510	.73897,-.25770E-1
.8	1.7298,-.36252	.68444,-.27817E-2
.84	1.8206,-.39118	.55456, .32677E-1
.88	1.9309,-.41243	.40176, .47700E-1
.9	1.9933,-.41842	.32101, .45619E-1

Figure 9

$R_1/R_2 = 0.78$, $Re = 100$, $\alpha R_2 = 1$, Mode 0

The first column tracks the interfacial eigenvalue c from its value at $\mu_1/\mu_2 = 1$ down to $\mu_1/\mu_2 = 0.2$.

The second column tracks a one-fluid eigenvalue c_{SG} recorded by Salwen and Grosch for $\mu_1/\mu_2 = 1$.

Truncation of Chebyshev polynomials is at NN = 19

$\frac{\mu_1}{\mu_2}$	c	c_{SG}
1.0	.39160, 0	.81160,-.28413
.9	.40351, .14598E-2	.86463,-.26774
.8	.41811, .32395E-2	.93120,-.25273
.7	.43647, .53647E-2	1.0161 ,-.24078
.6	.46035, .77833E-2	1.1288 ,-.23714
.5	.49279, .10166E-1	1.2929 ,-.26247
.4	.53954, .11271E-1	1.3296 ,-.35730
.35	.57159, .10191E-1	1.3926 ,-.36389
.3	.61257, .63780E-2	1.4675 ,-.36010
.2	.73897, .25770E-1	1.6906 ,-.34510

$R_1/R_2 = 0.6$, $Re = 100$, $\alpha R_2 = 1$, Mode 0

The interfacial eigenvalue c is tracked from its value at $\mu_1/\mu_2 = 1$ down to 0.2.

The one-fluid eigenvalue c_{SG} is tracked closely between $\mu_1/\mu_2 = 0.46$ and 0.2.

$\frac{\mu_1}{\mu_2}$	c	c_{SG}
1.0	.64 , 0	
.8	.67521,-.22710E-2	
.6	.73259,-.94479E-2	.92385,-.52808
.46	.79973,-.26749E-1	1.0639 ,-.40287
.44	.81229,-.31472E-1	1.0907 ,-.37493
.42	.82578,-.37217E-1	1.1173 ,-.33474
.4	.84021,-.44267E-1	1.1142 ,-.29304
.38	.85558,-.52993E-1	1.1175 ,-.27473
.35	.87994,-.70309E-1	1.1377 ,-.25073
.33	.89628,-.85488E-1	1.1584 ,-.23392
.3	.91806,-.11425	1.2022 ,-.20574
.28	.92884,-.13602	1.2423 ,-.18576
.25	.93956,-.16804	1.3218 ,-.15788
.23	.94509,-.18766	1.3887 ,-.14216
.2	.95413,-.21492	1.515 ,-.12375

Real (c) decreases with n and approaches $W(R_1)$ as $n \to \infty$ (see graph 12). Only for $R_1/R_2 \gtrsim 0.7$ was the configuration of minimum dissipation found to be stable. At $Re = 100$, $\alpha R_2 = 1$, compare $R_1/R_2 = 0.7, 0.8, 0.9$ (graphs 13, 6, 14). All modes have the same behaviour for $R_1/R_2 = 0.8, 0.9$; they are unstable if $\mu_1/\mu_2 < 1$ and stable if $\mu_1/\mu_2 > 1$. However, we find that for $\mu_1/\mu_2 < 1$ the zeroth mode can become stable, (see $Re = 100$, $R_1/R_2 = 0.2, 0.5$ or $R_1/R_2 = 0.8$, graphs 15, 16,6).

Large αR_2, moderate Re, $\mu_1/\mu_2 \in [0.2, 2]$

As αR_2 increases, the region of stability decreases.

Graphs 17 - 18 illustrate the variation with R_1/R_2 at $Re = 1$, $\alpha R_2 = 10$. Graphs 19 - 21, illustrate the variation with R_1/R_2 at $Re = 100$, $\alpha R_2 = 10$. In practice, surface tension may dampen the instabilities as in the case of flow down an inclined plane (Yih, p. 502). For small α, Hickox showed that surface tension effects are negligible except when $R_1/R_2 \lesssim 0.1$. The real (c) for all modes lie close together. See Graph 22.

Larger Re. At $Re = 1000$, $R_1/R_2 = 0.8$, $\alpha R_2 = 1$, graph 23 (compare with graph 6) shows that stability is lost via the 0^{th} mode.

Larger μ_1/μ_2 The variation of im (c) with μ_1/μ_2 larger than 2 for given α and R_1/R_2 is less rapid than for smaller μ_1/μ_2. See graphs 24-26 for $Re = 100$, $\alpha R_2 = 1$, $R_1/R_2 = 0.5$, and $Re = 100$, $\alpha R_2 = 1$, $R_1/R_2 = 0.9$ and $Re = 100$, $\alpha R_2 = 10$, $R_1/R_2 = 0.9$.

The experiments reported by Everage [2] are for $\mu_1/\mu_2 \approx 6$ and equal volume fluxes, from which we compute $R_1/R_2 = 0.57$. This value also agrees with his photograph. Calculations in Graph 24 show that for $\mu_1/\mu_2 > 4$, Im c changes very little. It follows from our calculations (graph 24) that the concentric configuration, in the experiment of Everage, should be unstable. However, the growth rates of the unstable modes are very small, so instabilities may take a longer time to develop than the observation time in Everage's experiment. It is also possible that the instability only grows to a small amplitude, and the eventual flow might not be very different from the concentric pattern.

In the case where R_1/R_2 is large, as would be the case in "lubrication" applications such as oil transport, we find that concentric encapsulation is the preferred configuration.

GRAPH 1

Imaginary part of c versus viscosity ratio

Re = 1, αR_2 = 0.1, R_1/R_2 = .0.6

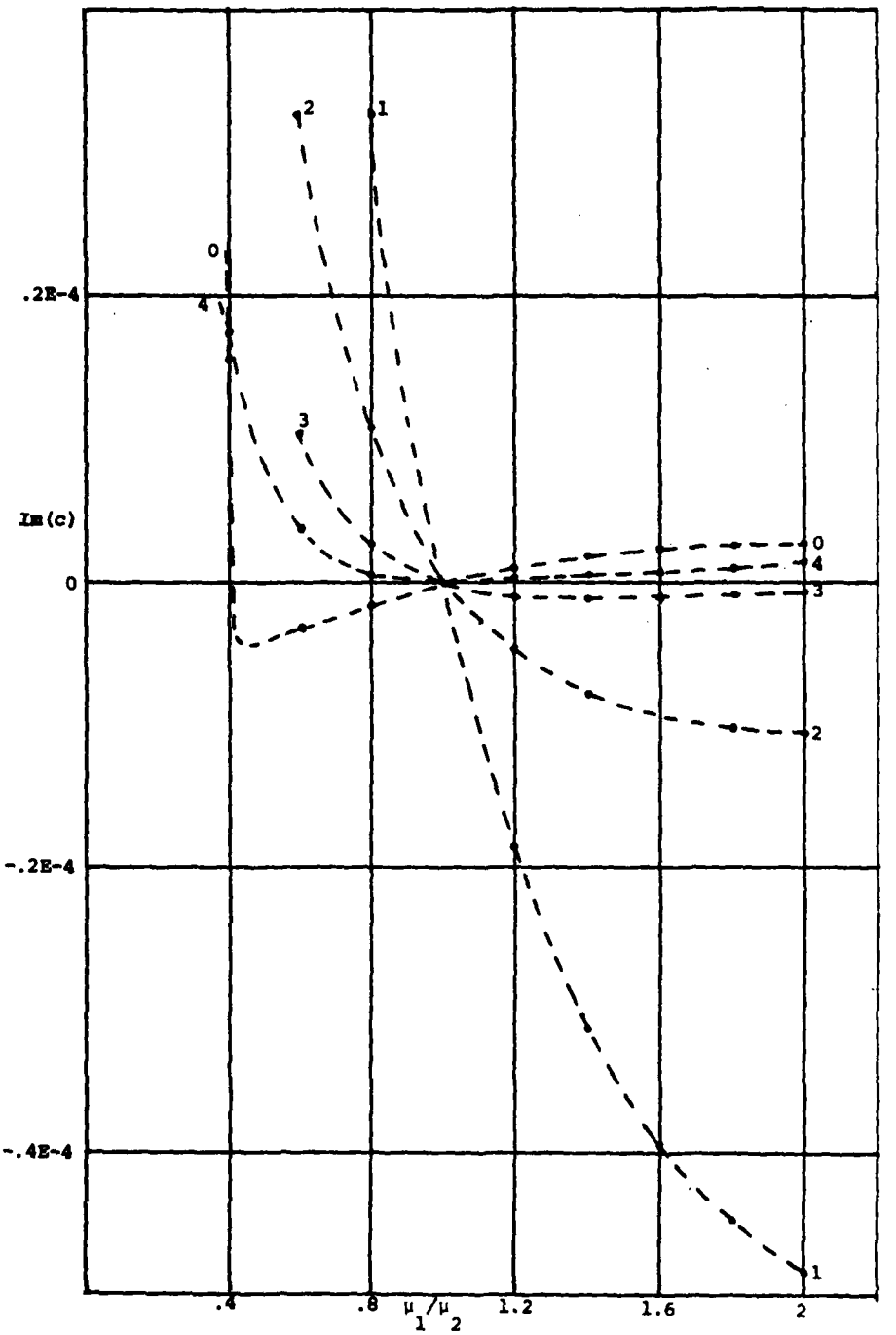

GRAPH 2

Imaginary part of c versus viscosity ratio

Re = 1, αR_2 = 1, R_1/R_2 = 0.6

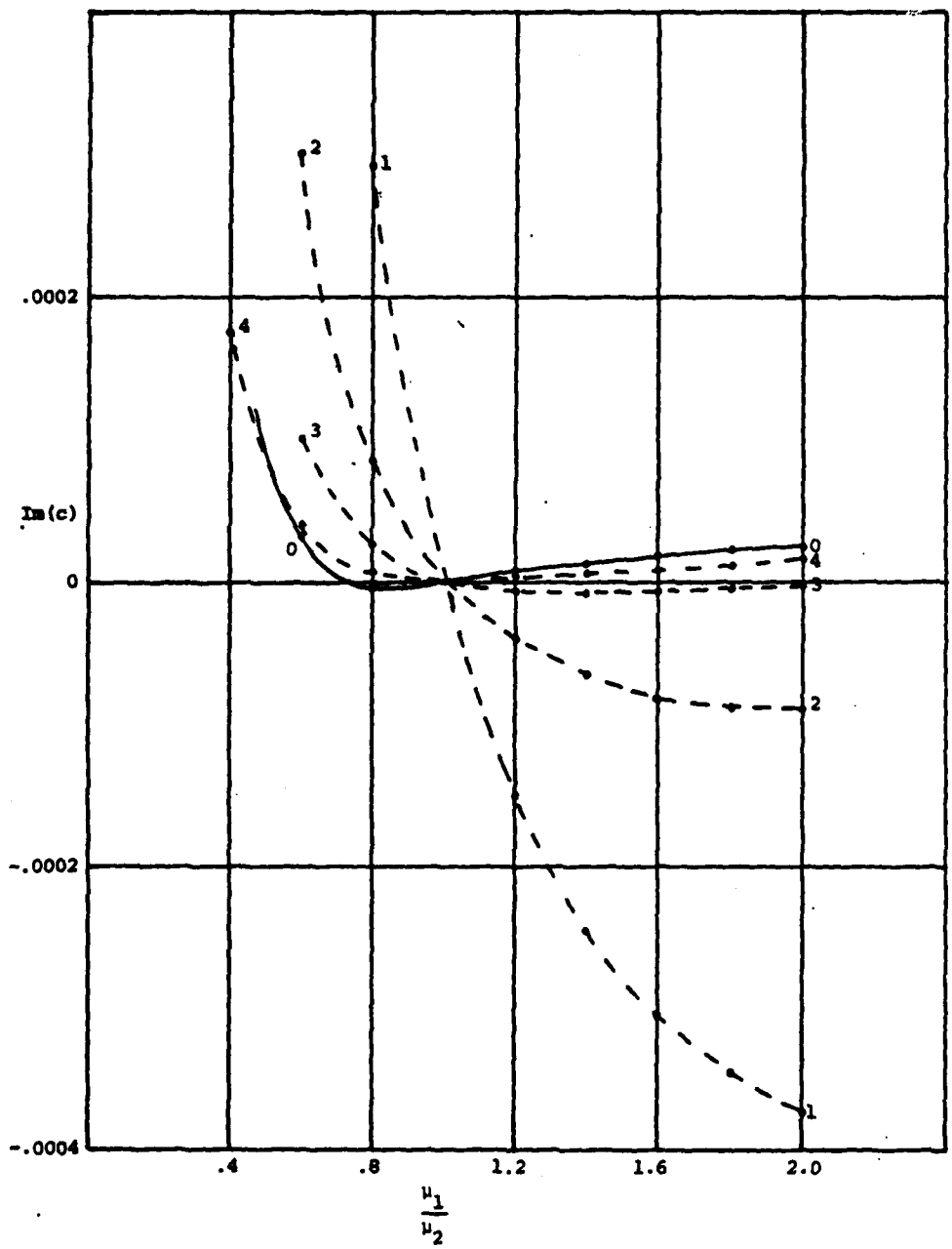

GRAPH 3

Imaginary part of c versus viscosity ratio

Re = 10, αR_2 = 1, R_1/R_2 = 0.6

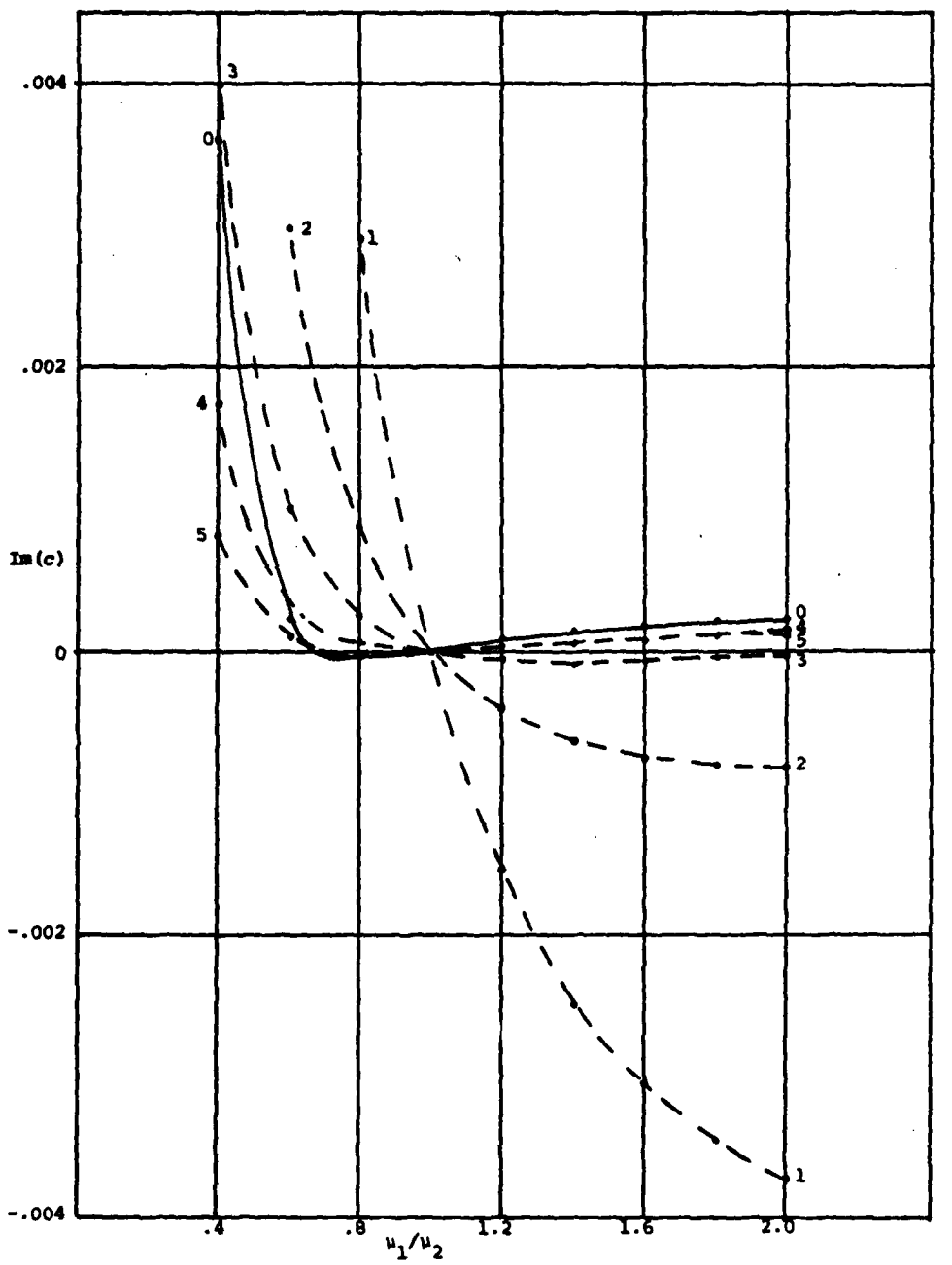

GRAPH 4

Re = 100, $\alpha R_2 = 1$, $R_1/R_2 = 0.6$

Magnification on the right shows behaviour for $1 \leq \frac{\mu_1}{\mu_2} \leq 2$

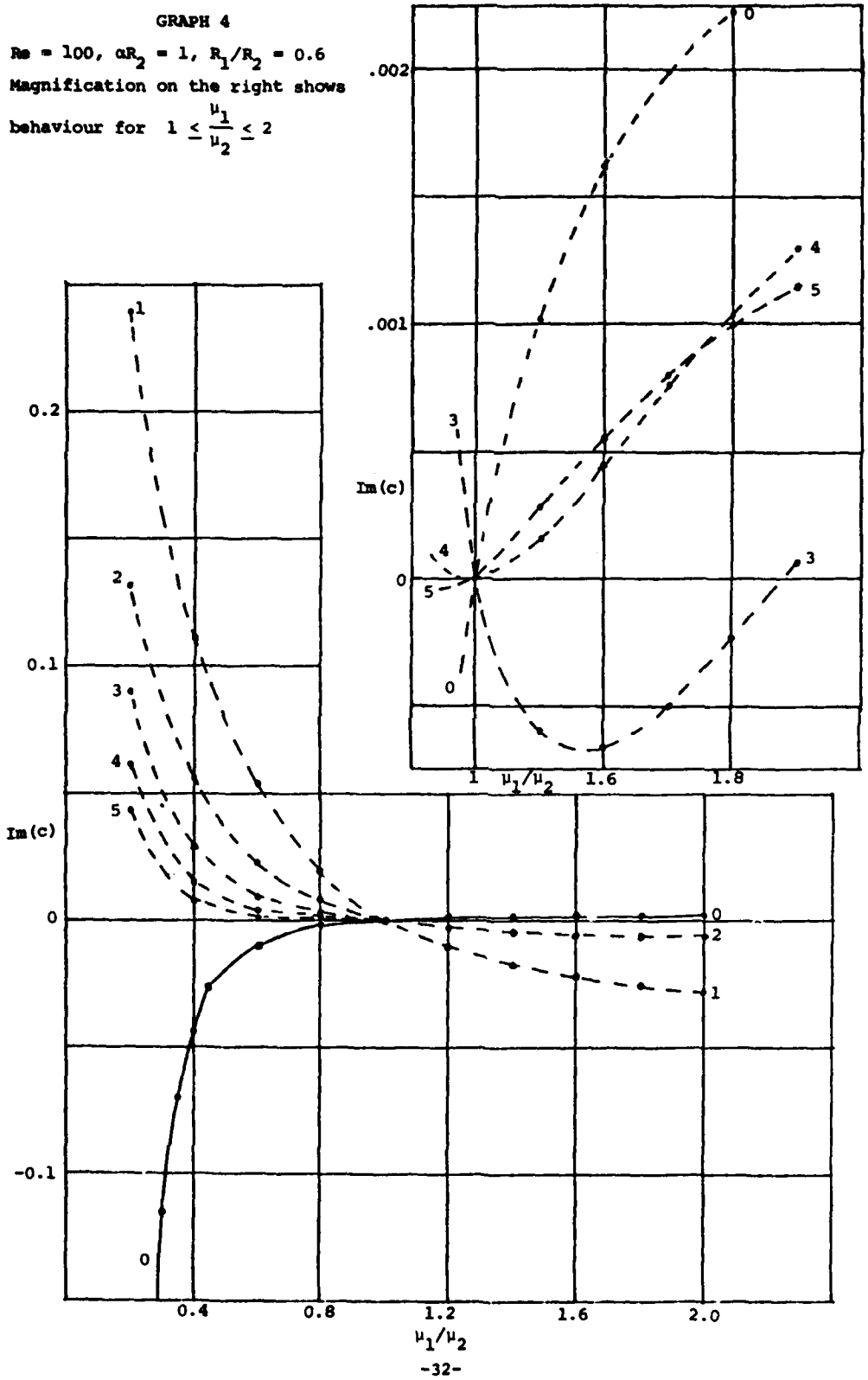

GRAPH 5

Imaginary part of c versus viscosity ratio for
low Reynolds number and moderate α.

$Re = 1,\ \alpha R_2 = 1,\ R_1/R_2 = 0.8$

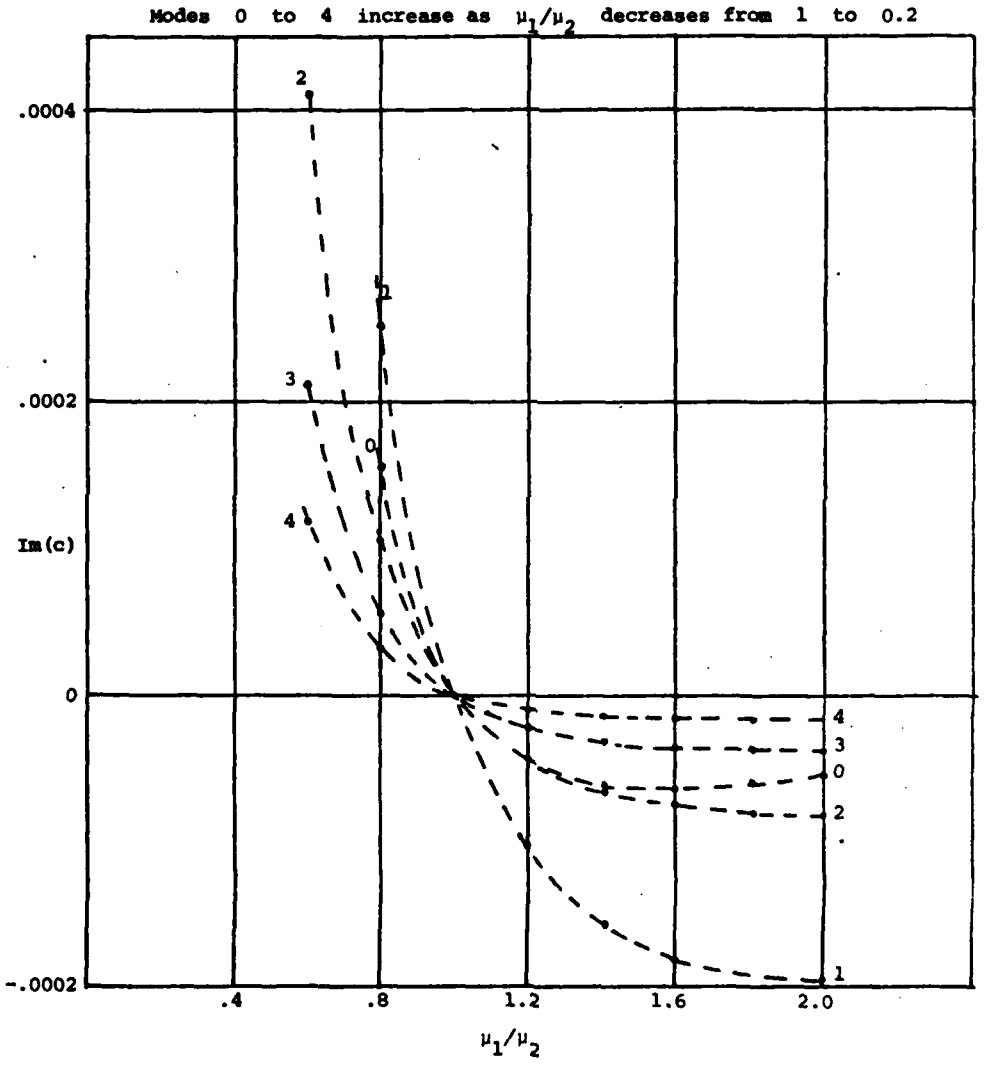

GRAPH 6

Re = 100, $R_2 = 1$, $R_1/R_2 = 0.8$

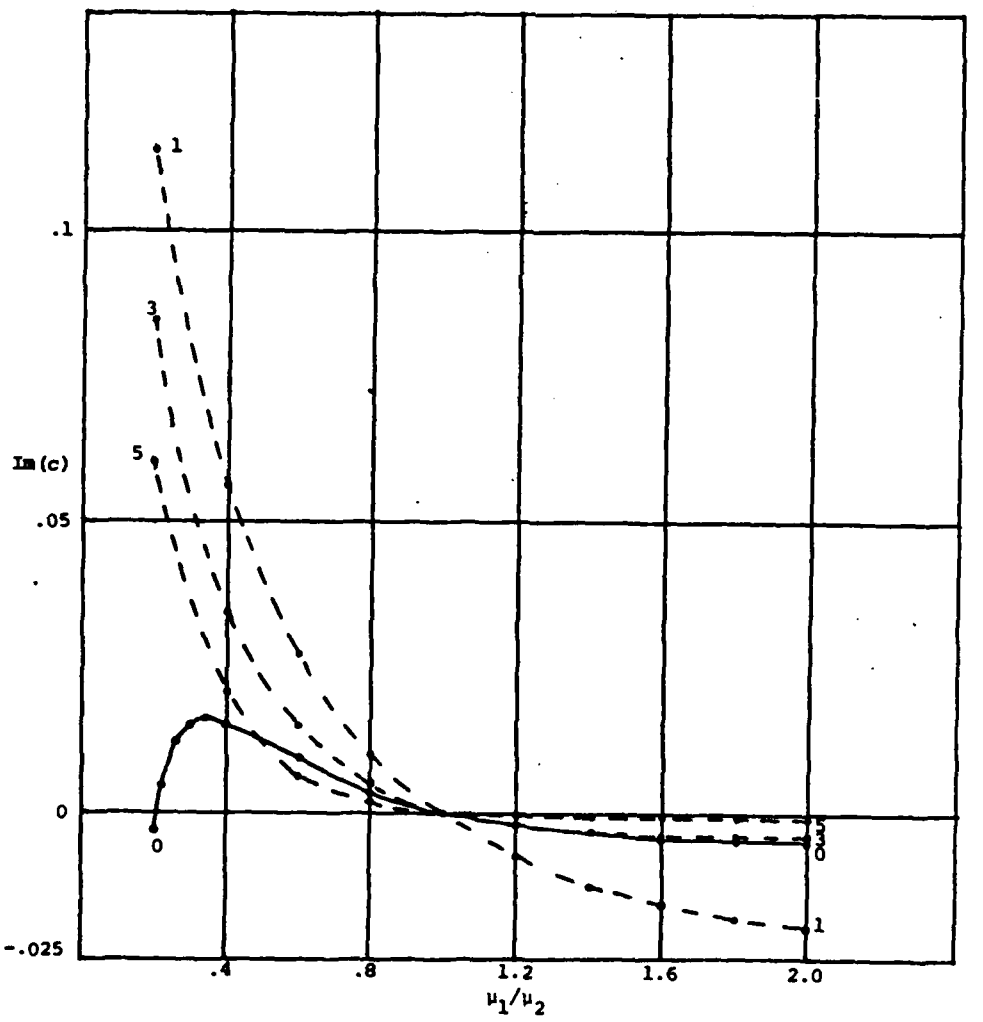

GRAPH 7

Re = 100, αR_2 = 1, mode 0

Numerals next to the curves denote μ_1/μ_2.

The curves for $\frac{\mu_1}{\mu_2}$ = 1.6 to 2.0 are identical under graph scales.

Refer to §§5 for comments on $\frac{\mu_1}{\mu_2}$ = 0.2.

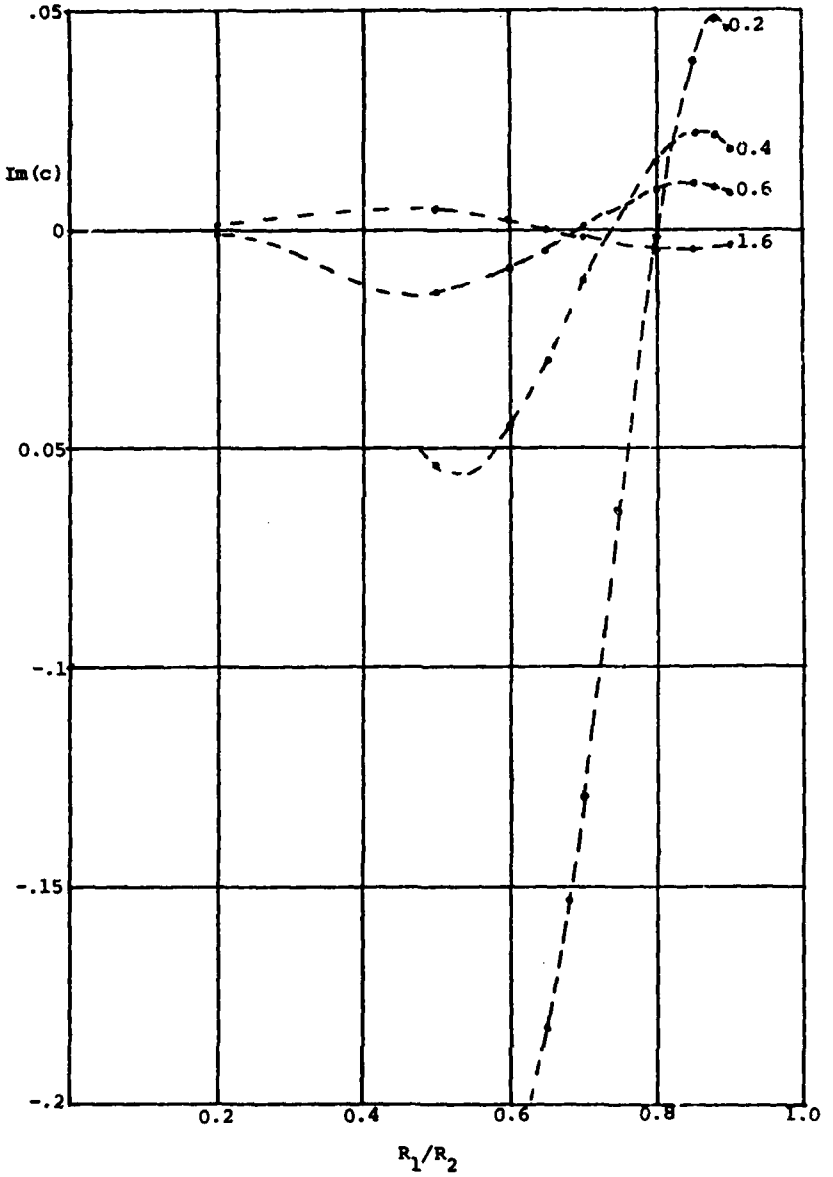

GRAPH 8

$Re = 100$, $\alpha R_2 = 1$, mode 1

Numbers next to curves denote $\frac{\mu_1}{\mu_2}$.

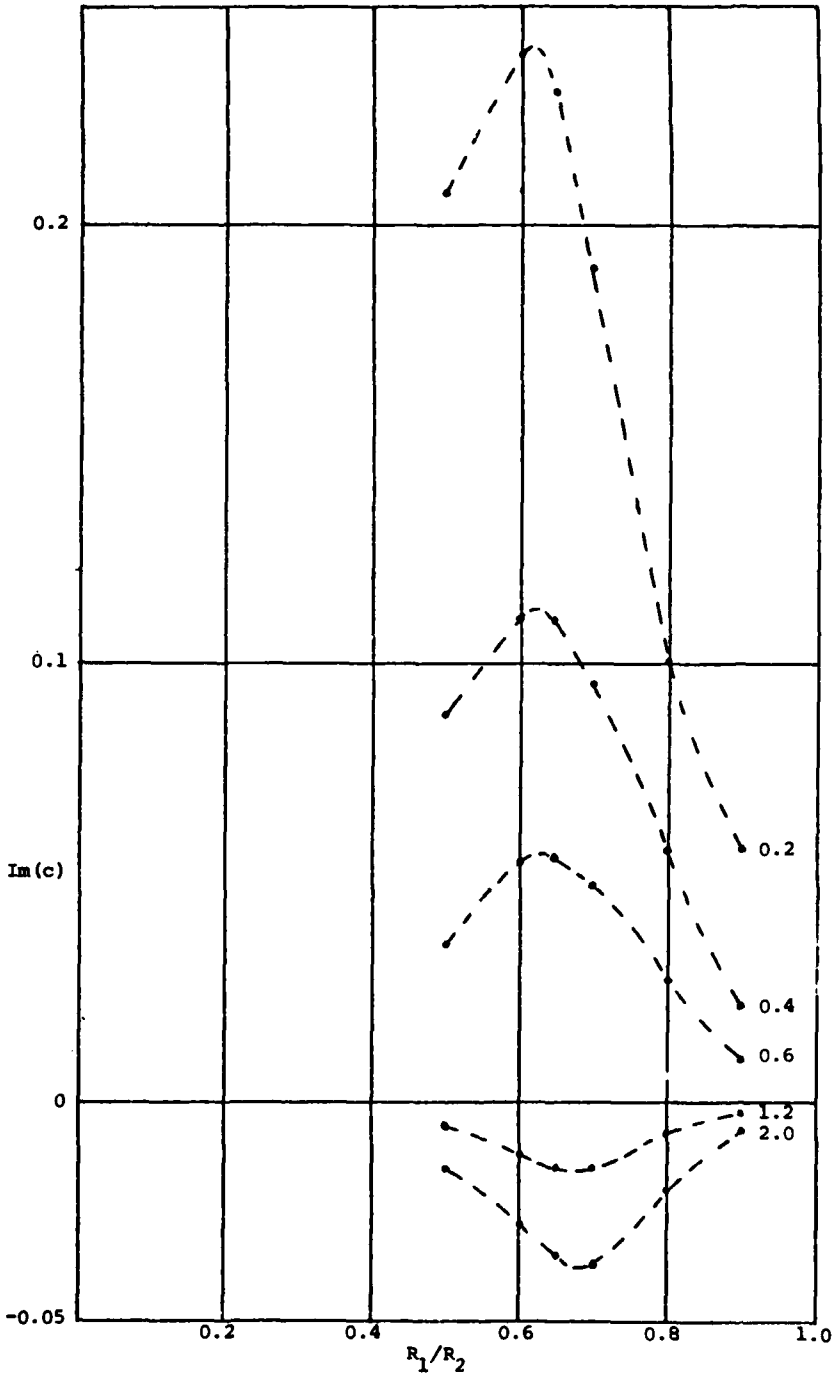

GRAPH 9

Re = 100, αR_2 = 1, mode 2

Numerals next to curves denote $\frac{\mu_1}{\mu_2}$.

The curves for $\frac{\mu_1}{\mu_2}$ = 1.6 to 2.0 are indistinguishable under these scales.

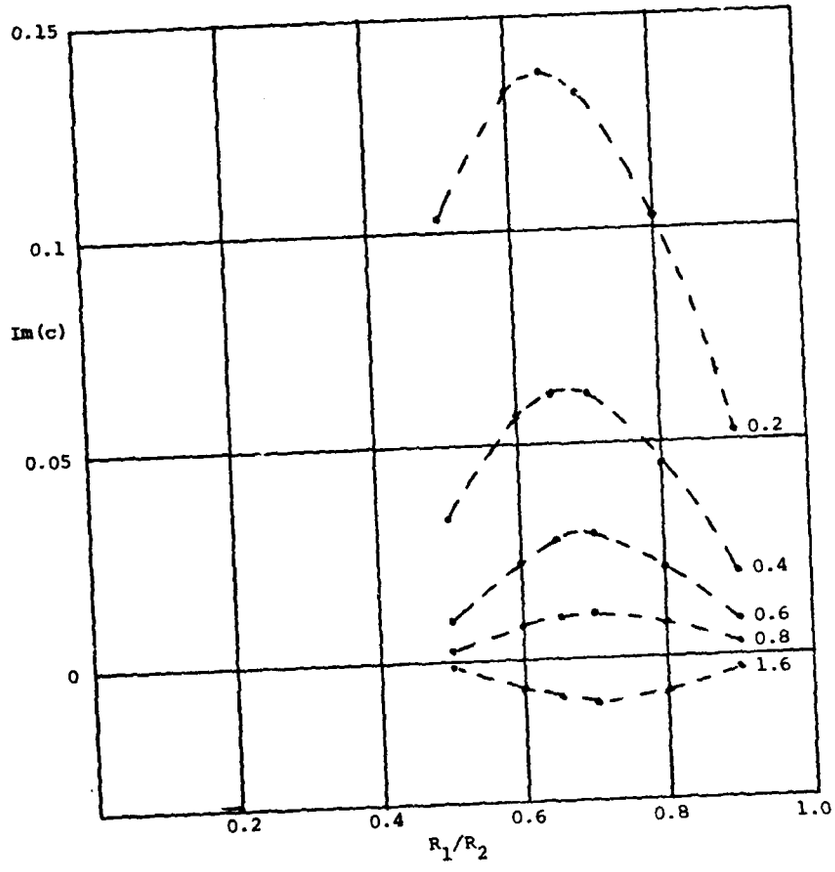

GRAPH 10

Re = 100, αR_2 = 1, mode 3

Ratios next to curves denote $\frac{\mu_1}{\mu_2}$.

The curves for $\frac{\mu_1}{\mu_2}$ = 1.4 to 2.0 are indistinguishable under these scales

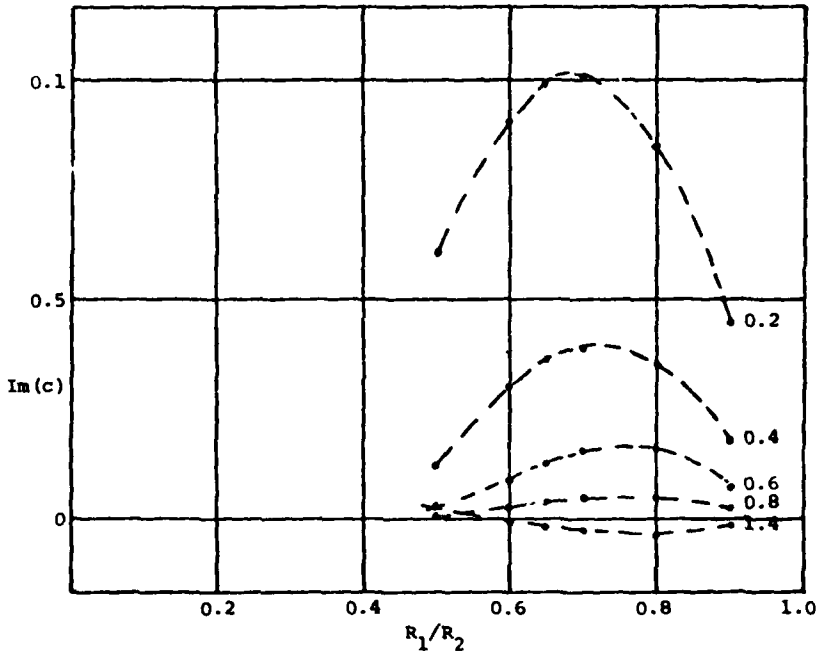

GRAPH 11

Re = 100, αR_2 = 1, mode 4

Numerals next to curves denote $\frac{\mu_1}{\mu_2}$.

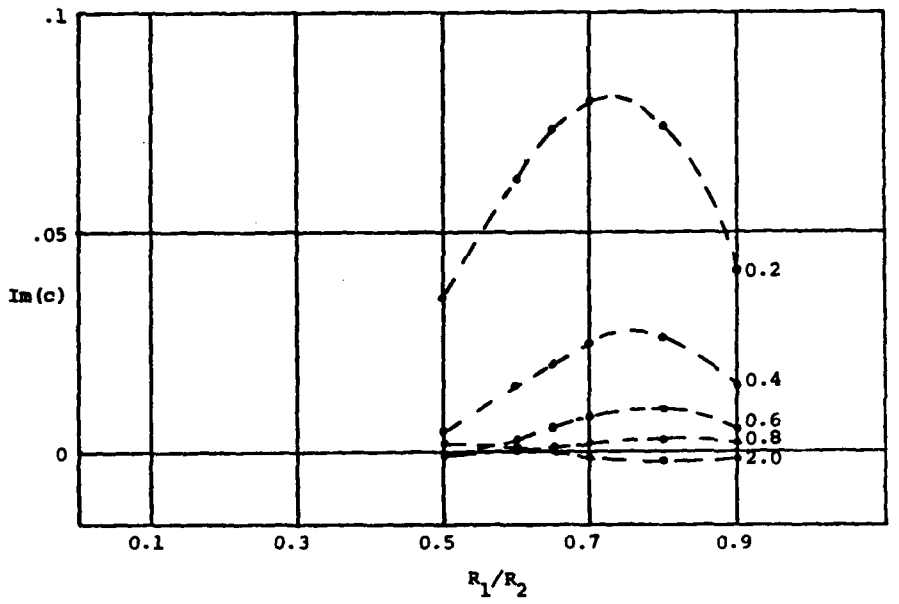

GRAPH 12

Real part of c versus viscosity ratio.

Re = 10, αR_2 = 1, R_1/R_2 = 0.6, velocity scale = 1

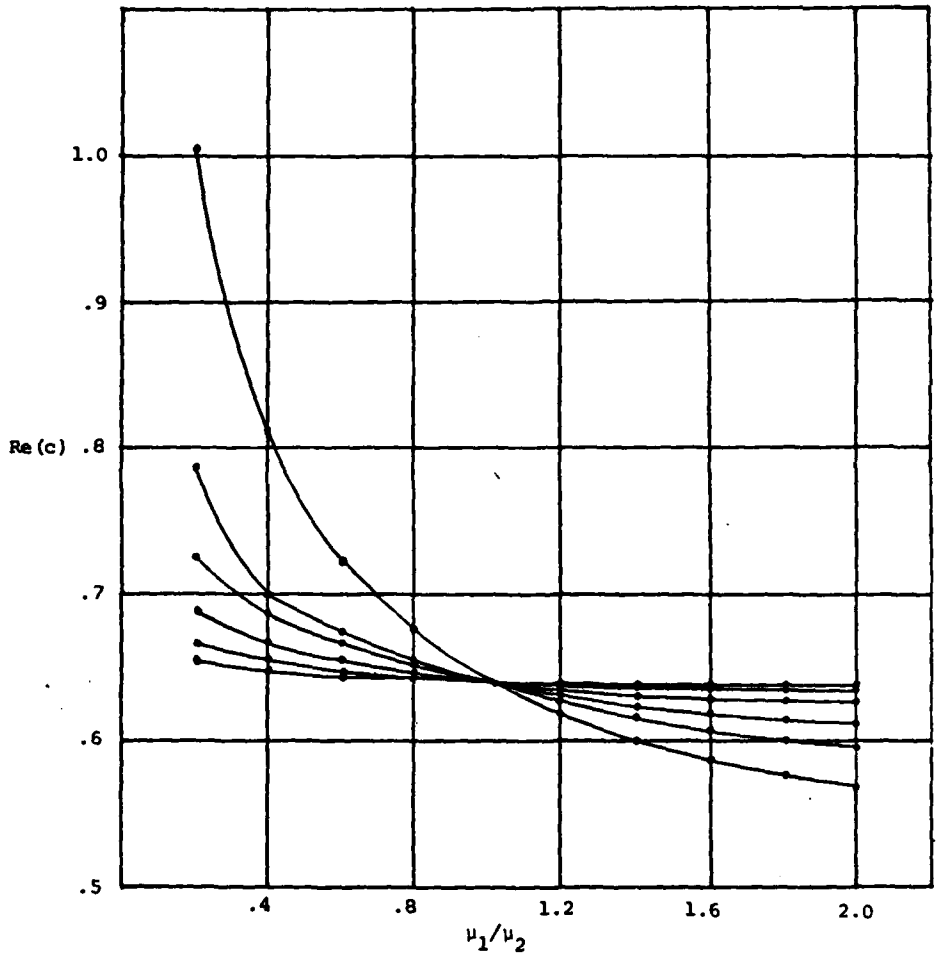

GRAPH 13

Re = 100, $\alpha R_2 = 1$, $R_1/R_2 = 0.7$.

The magnification on the right displays behaviour for $1 \leq \frac{\mu_1}{\mu_2} \leq 2$.

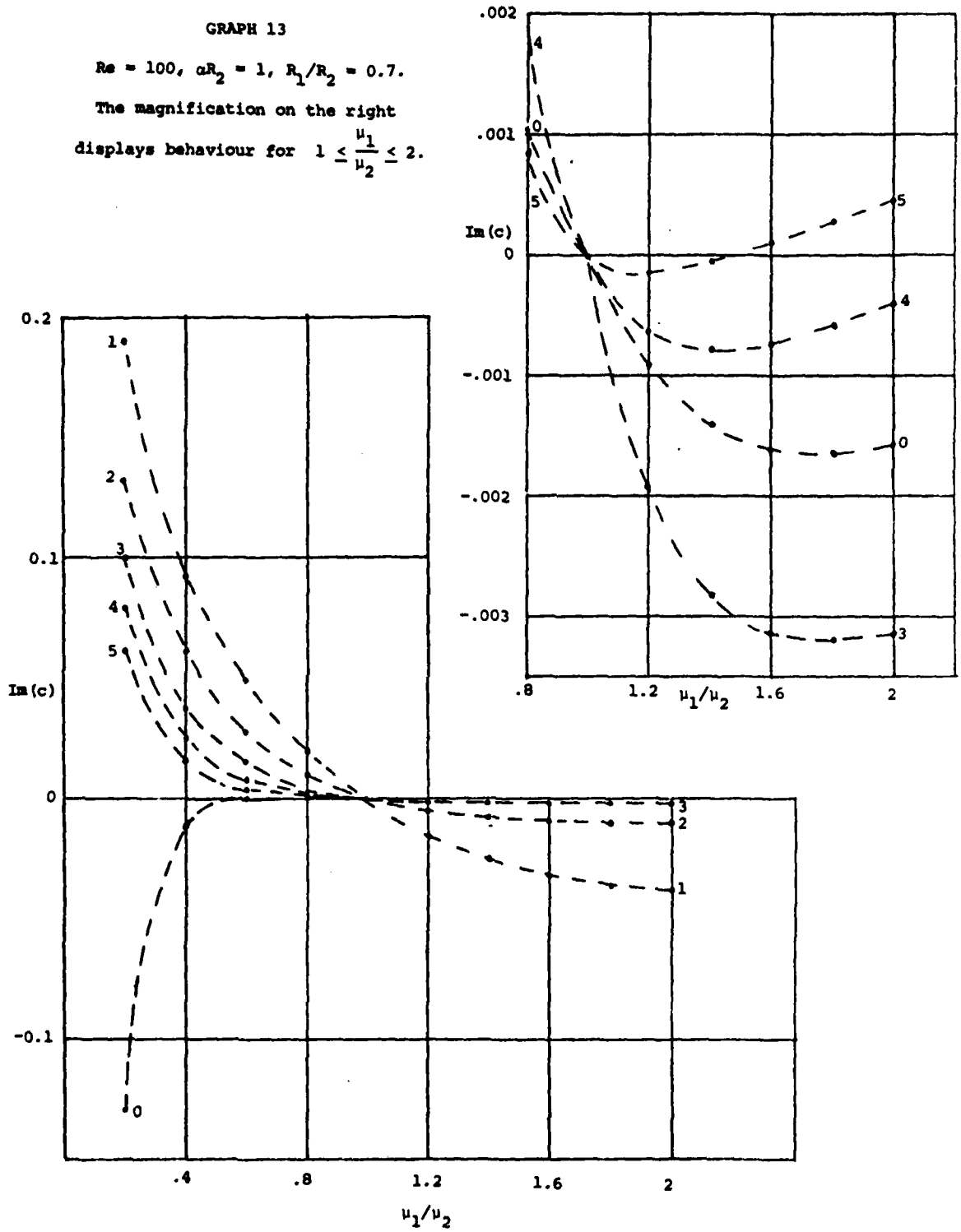

GRAPH 14

Re = 100, R_1/R_2 = 0.9, αR_2 = 1, velocity scale = 1

Curve for mode 3 lies between modes 2 and 4

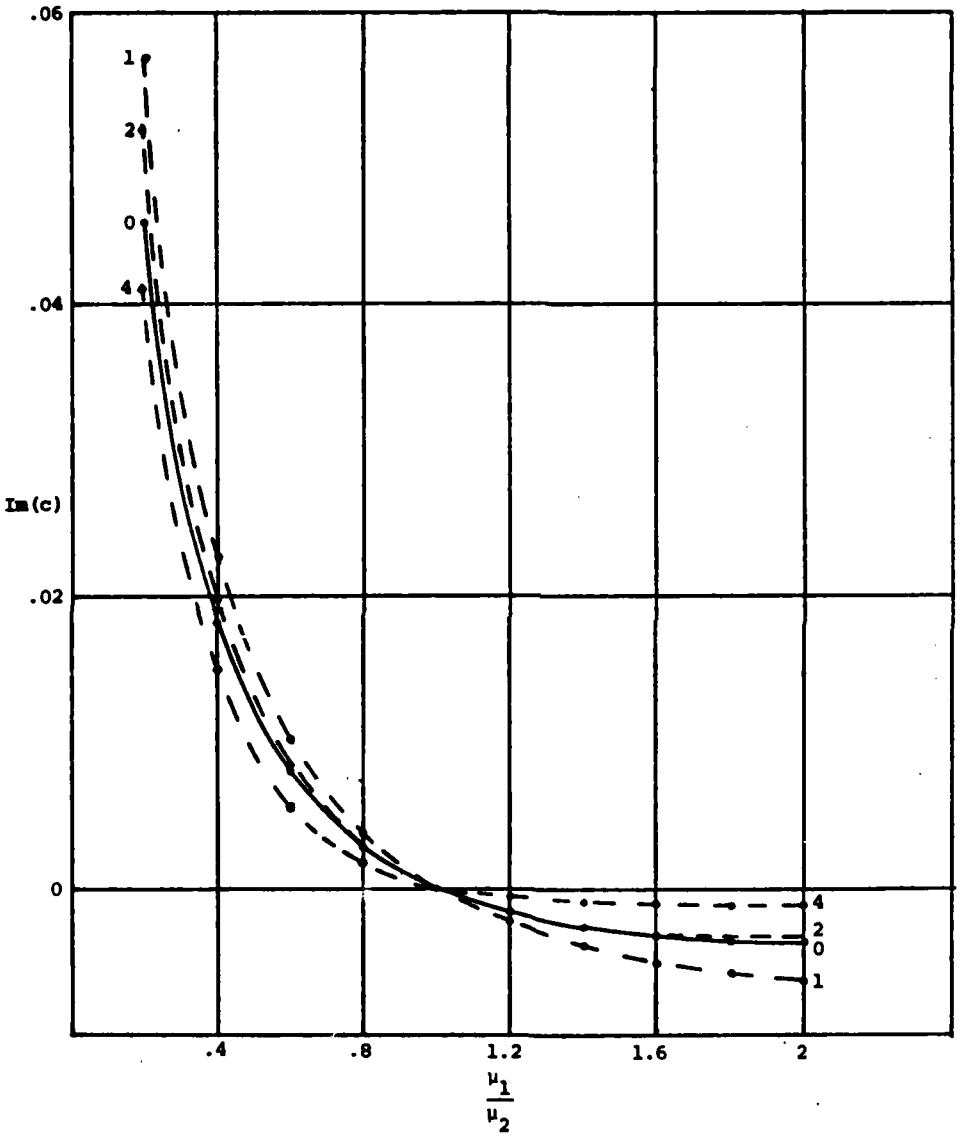

GRAPH 15

Imaginary part of c versus viscosity ratio

Re = 100, αR_2 = 1, R_1/R_2 = 0.2, velocity scale = 1

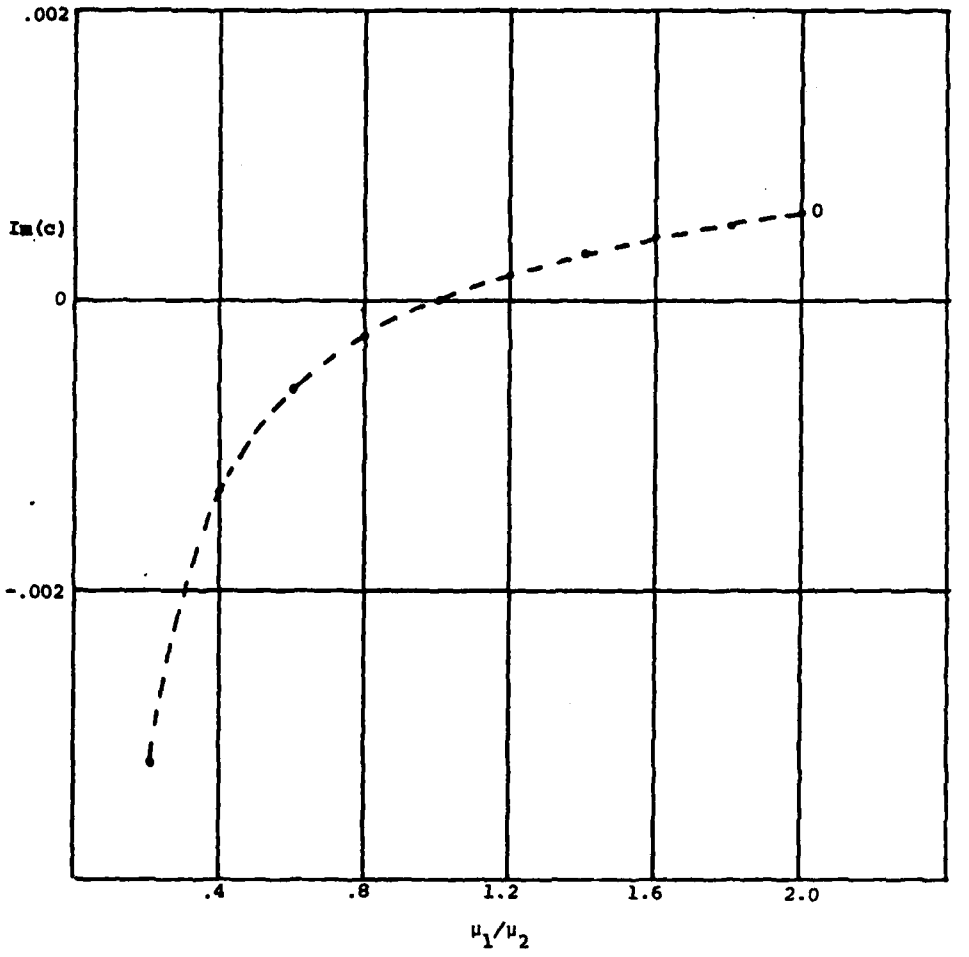

GRAPH 16

Re = 100, $\alpha R_2 = 1$, $R_1/R_2 = 0.5$

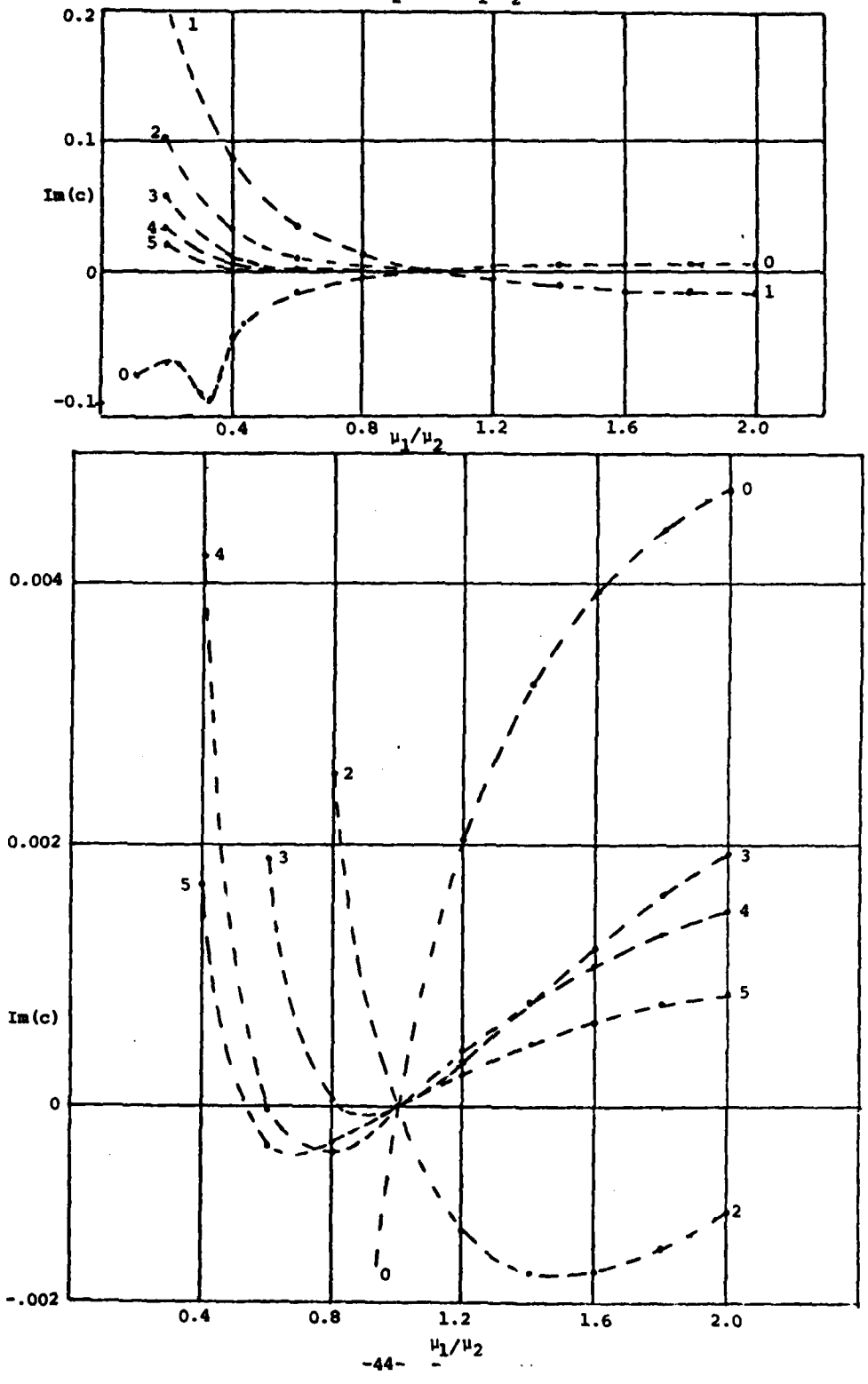

GRAPH 17

Imaginary part of c versus viscosity ratio for large α and low Reynolds number

Re = 1, αR_2 = 10, R_1/R_2 = 0.6

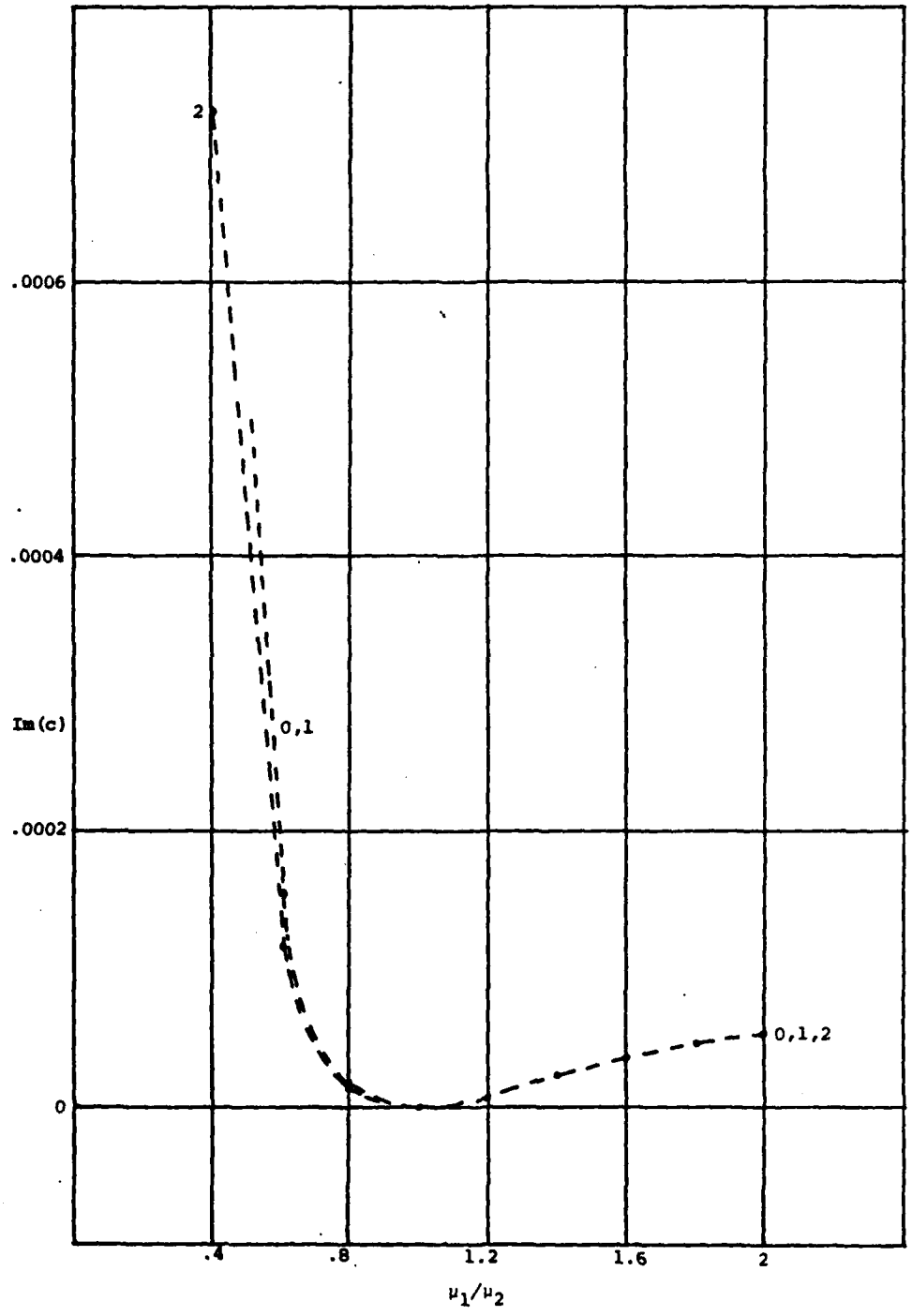

GRAPH 18

Imaginary part of c versus viscosity ratio for large α and low Reynolds number

$Re = 1$, $\alpha R_2 = 10$, $R_1/R_2 = 0.8$

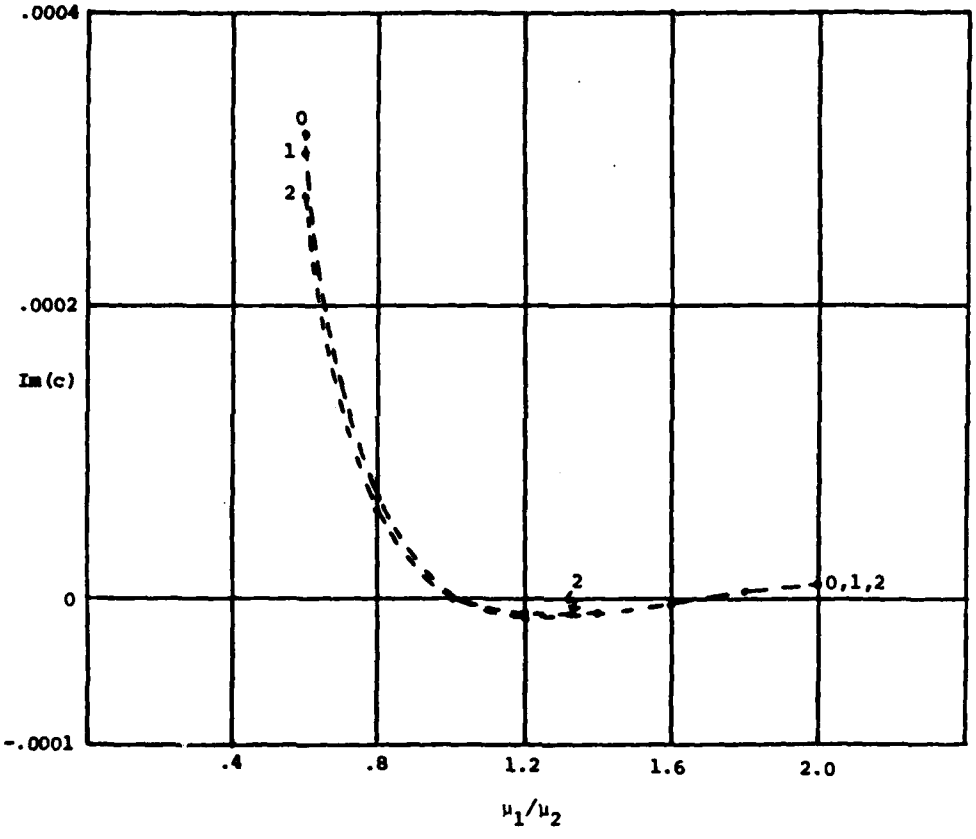

GRAPH 19: Re = 100, αR_2 = 10, R_1/R_2 = 0.6.

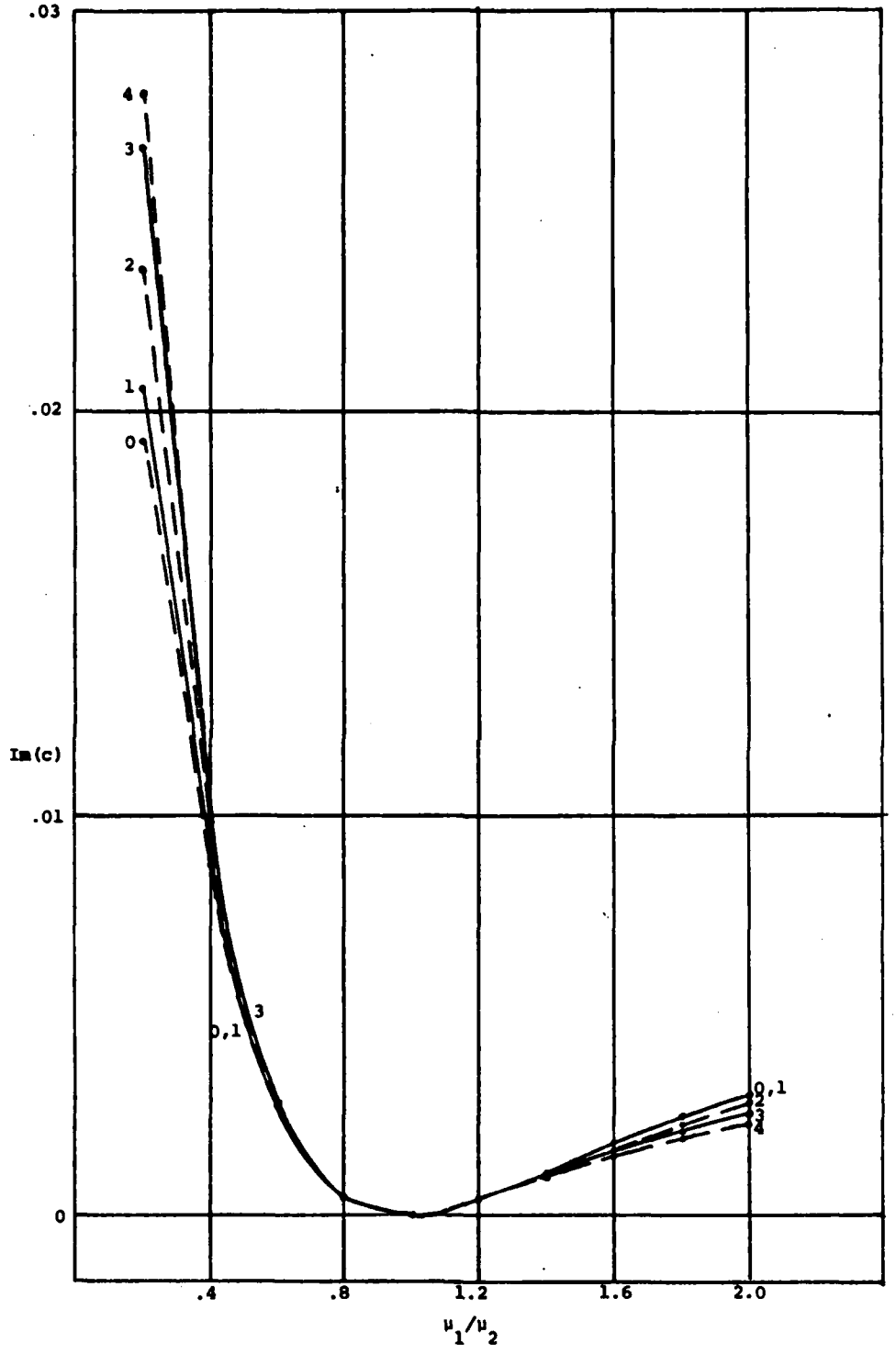

GRAPH 20: Re = 100, αR_2 = 10, R_1/R_2 = 0.8

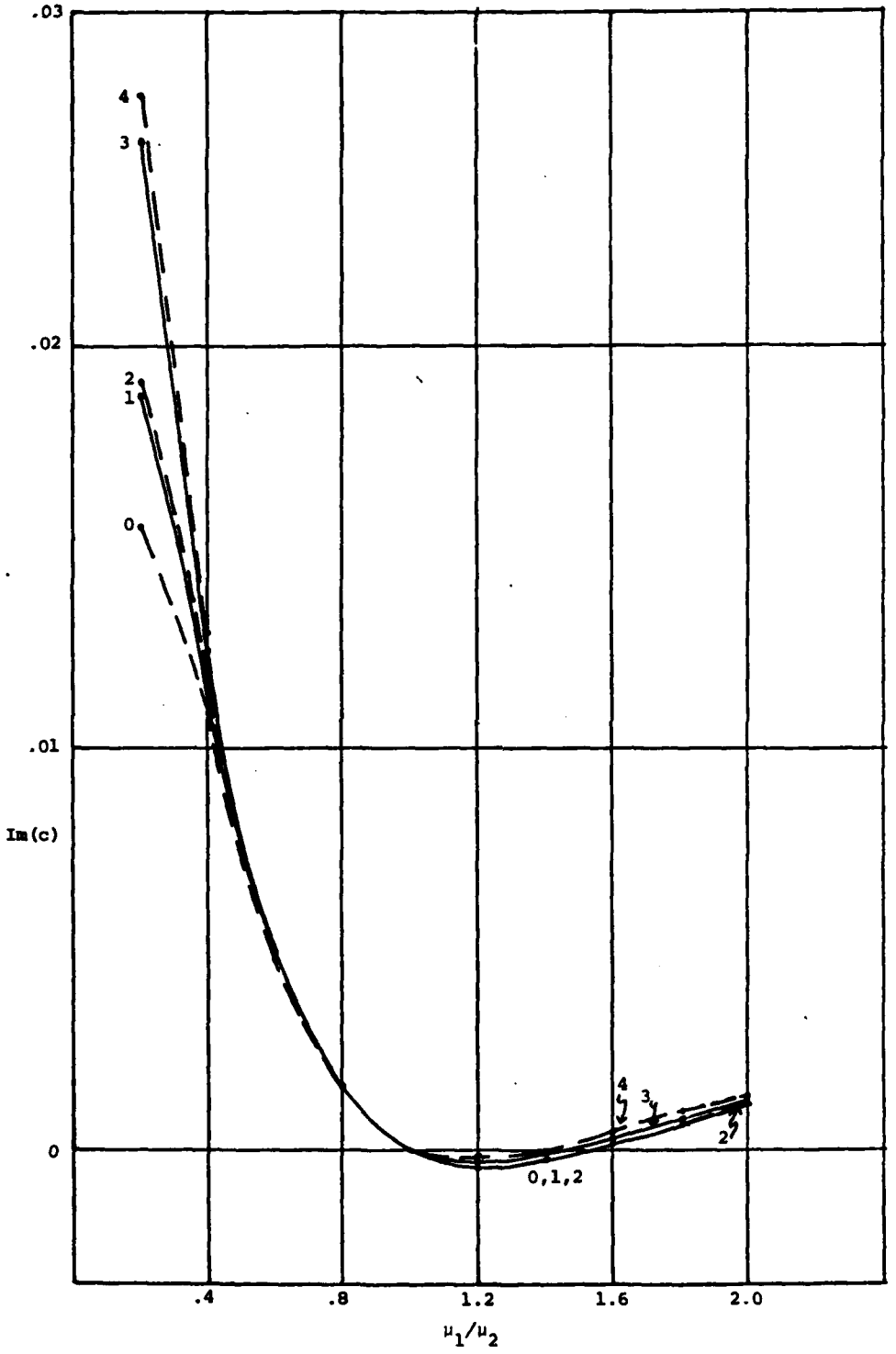

GRAPH 21: Re = 100, αR_2 = 10, R_1/R_2 = 0.9
Imaginary part of c versus μ_1/μ_2 for large α

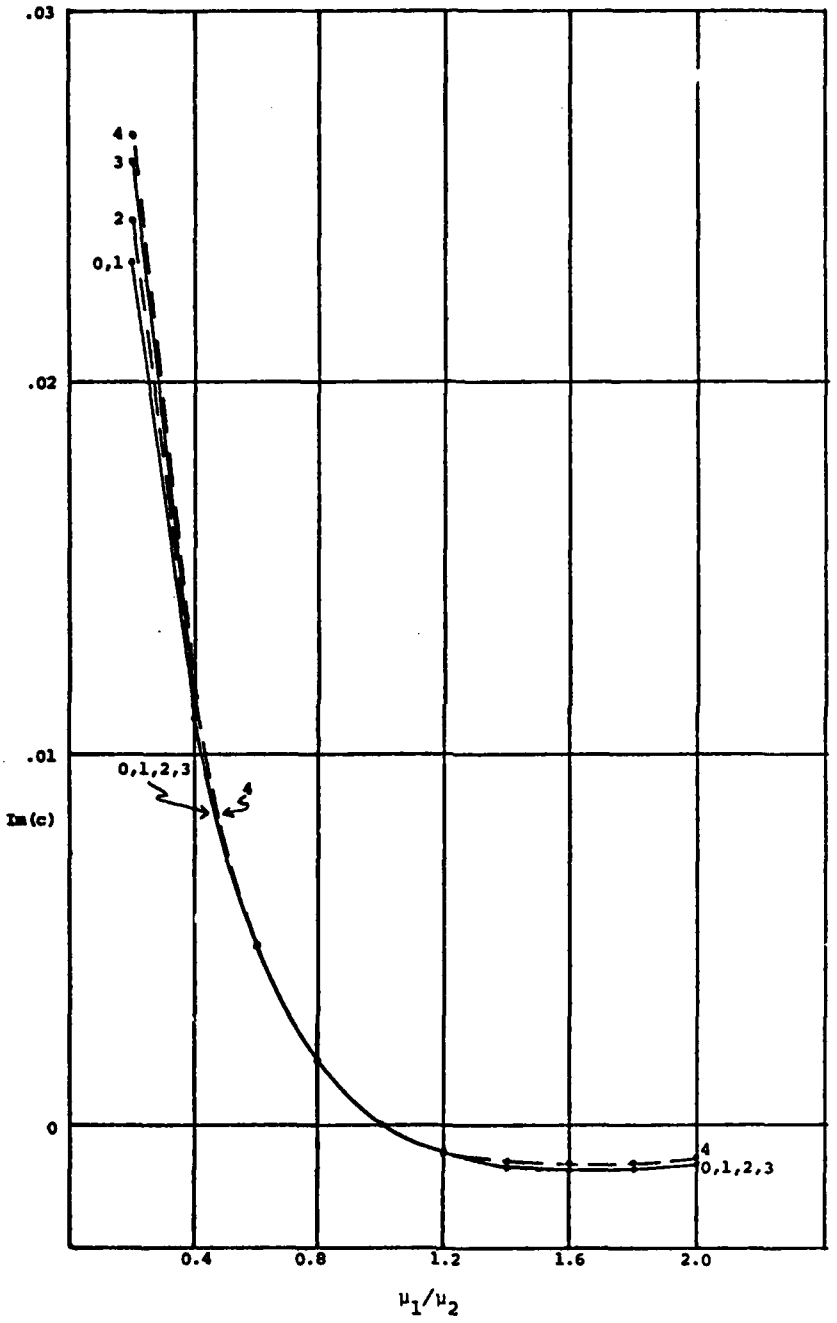

GRAPH 22

Real part of c versus viscosity ratio

Re = 100, R_1/R_2 = 0.6, αR_2 = 10, velocity scale = 1

Curves for modes 1, 2 and 3 lie between modes 0 and 4

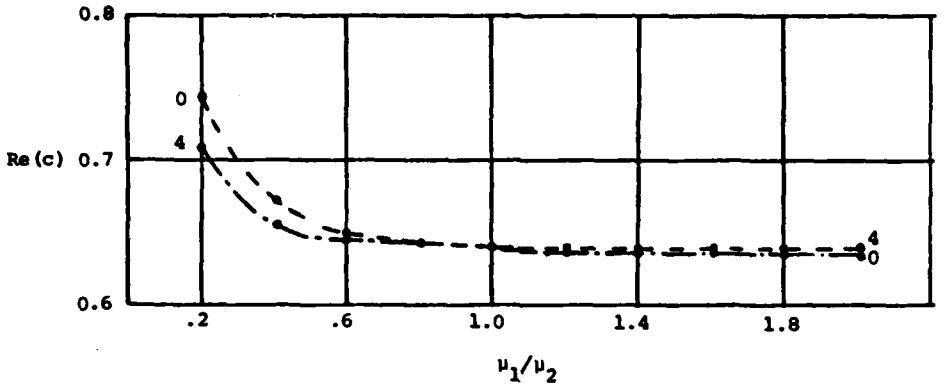

GRAPH 23

Imaginary part of c versus viscosity ratio

Re = 1000, αR_2 = 1, R_1/R_2 = 0.8, velocity scale = 1

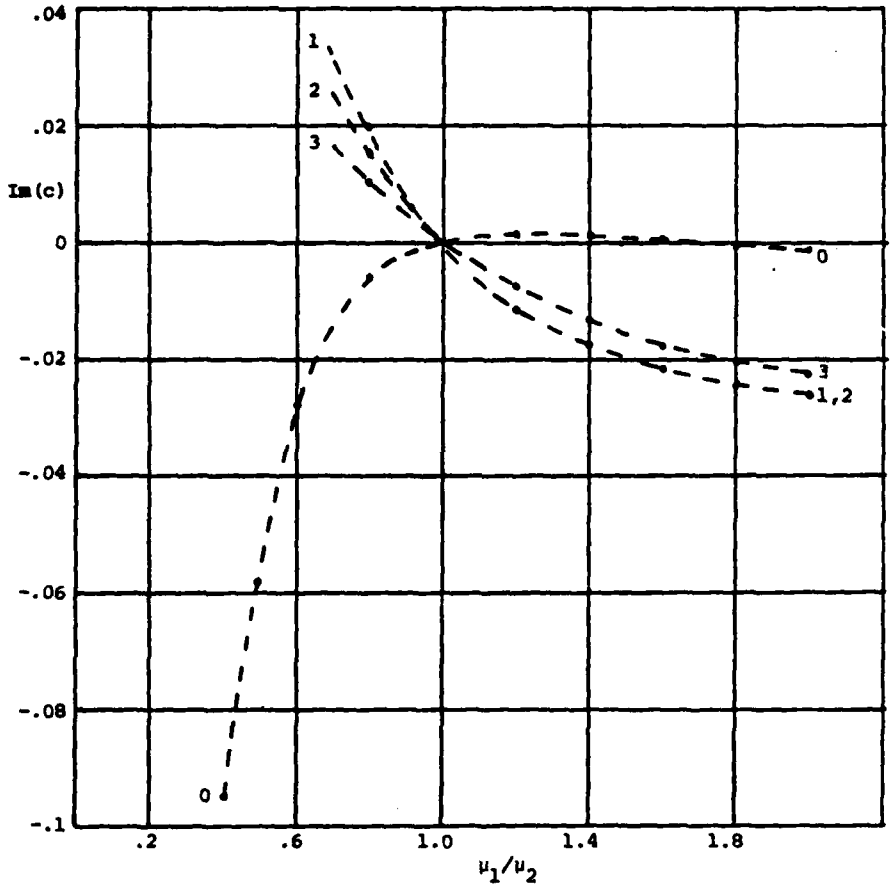

GRAPH 24

$Re = 100,\ \alpha R_2 = 1,\ R_1/R_2 = 0.5$

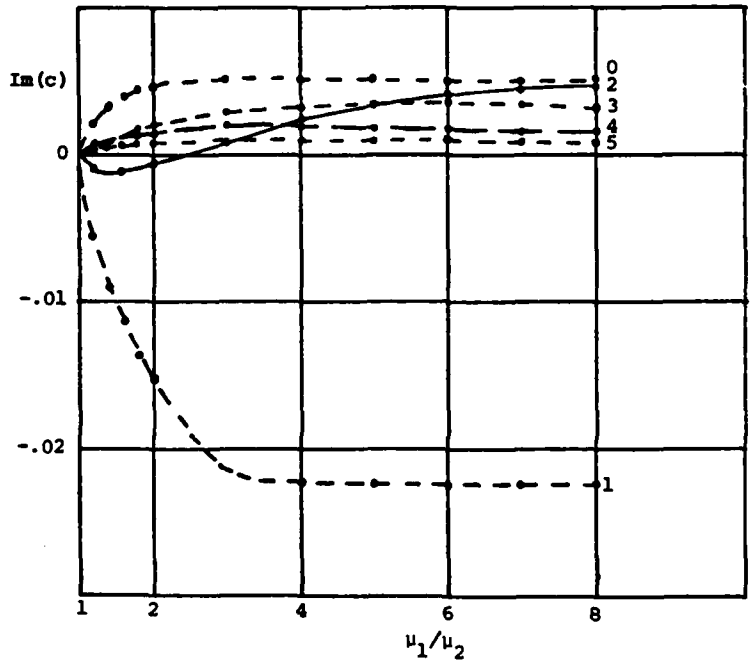

GRAPH 25

Re = 100, $\alpha R_2 = 1$, $R_1/R_2 = 0.9$

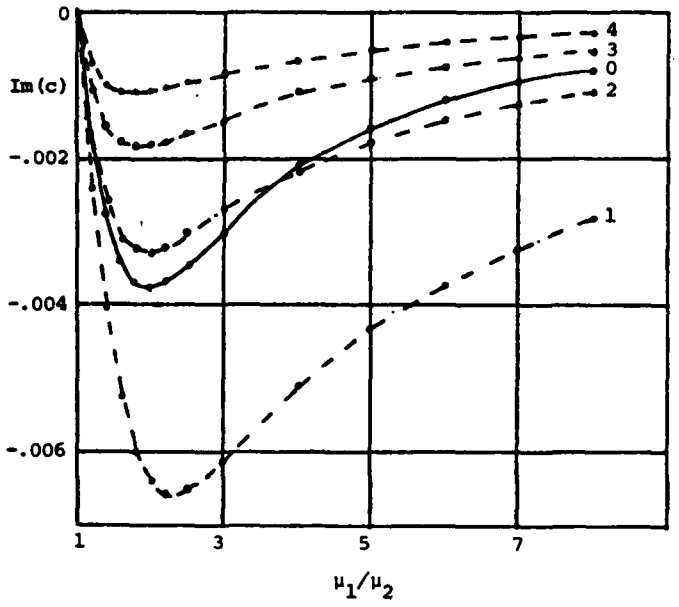

GRAPH 26

Re = 100, R_1/R_2 = 0.9, αR_2 = 10

"Large α" and "large μ_1/μ_2" regime.

Modes 0 to 4 have the same behaviour.

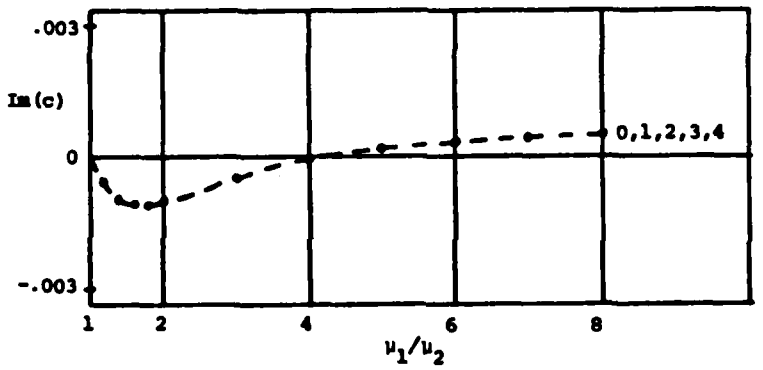

REFERENCES

[1] Charles, M. E. and Redberger, R. J., The Reduction of Pressure Gradients in Oil Pipelines by the Addition of Water. Numerical Analysis of Stratified Flows. Canadian J. Che. Eng. 40, 70-75 (1962).

[2] Everage, A. E. Jr., Theory of Bicomponent Flow of Polymer Melts. I. Equilibrium Newtonian Tube Flow, Trans. Soc. Rheology 17:4, 629-646 (1973).

[3] Hasson, D. and Mir, A., Annular Flow of Two Immiscible Liquids. II. Analysis of Core-Liquid Ascent, Canadian J. Chem. Eng. 48, 521-526 (1970).

[4] Hickox, Charles E., Instability Due to Viscosity and Density Stratification in Axisymmetric Pipe Flow, Physics of Fluids, 14, 251-262 (1971).

[5] Joseph, D. D., Nguyen, K. and Beavers, G. S., Nonuniqueness and Stability of the Configuration of Flow of Immiscible Fluids with Different Viscosities, to appear.

[6] MacLean, D. L., A Theoretical Analysis of Bicomponent Flow and the Problem of Interface Shape. Trans. Soc. Rheol. 17:3, 385-399 (1975).

[7] Minagawa, N. and White, J. L., Co-Extrusion of Unfilled and TiO_2-Filled Polyethylene: Influence of Viscosity and Die Cross-Section on Interface Shape. Polymer Engineering and Science, 15, 825-830 (1975).

[8] Orszag, S. A. and Kells, L. C., Transition to Turbulence in Plane Poiseuille and Plane Couette Flow, J. Fluid Mech. 96, 159-205 (1980).

[9] Salwen, H. and Grosch, C. E., The Stability of Poiseuille Flow in a Pipe of Circular Cross-Section, J. Fluid Mech. 54, 93-112 (1972).

[10] Salwen, H., Cotton, F. W. and Grosch, C. E., Linear Stability of Poiseuille Flow in a Circular Pipe, J. Fluid Mech. 98, 273-284 (1980).

[11] Southern, J. H. and Ballman, R. L., Stratified Bicomponent Flow of Polymer Melts in a Tube. Appl. Polymer Symp. No. 20, 175-189 (1973).

[12] White, J. L. and Lee, Biing-Lin, Theory of Interface Distortion in Stratified Two-Phase Flow. Trans. Soc. Rheology, 19:3, 457-479 (1975).

[13] Williams, M. C., Migration of Two Liquid Phases in Capillary Extrusion: An Energy Interpretation. AICHE Journal, 21, 1204-1207 (1975).

[14] Yih, C. S., Instability Due to Viscosity Stratification, J. Fluid Mech. 27, 337-352 (1967).

[15] Yu, H. S. and Sparrow, E. M., Experiments on Two-Component Stratified Flow in a Horizontal Duct. J. Heat Transfer, 91, 51-58 (1969).

DDJ/MR/YR/jvs